RSC Advances

PAPER

View Article Online
View Journal | View Issue

Cite this: *RSC Adv.*, 2021, **11**, 27226

Metabolome profiling and molecular docking analysis revealed the metabolic differences and potential pharmacological mechanisms of the inflorescence and succulent stem of *Cistanche deserticola*†

Xiao Sun,[ab] Yan Zheng,[abc] Lixia Tian,[ab] Yujing Miao,[ab] Tiexin Zeng,[abd] Yuan Jiang,[ab] Jin Pei,[d] Bashir Ahmad[e] and Linfang Huang *[ab]

Cistanche deserticola is an endangered plant used for medicine and food. Our purpose is to explore the differences in metabolism between inflorescences in non-medicinal parts and succulent stems in medicinal parts in order to strengthen the application and development of the non-medicinal parts of *C. deserticola*. We performed metabolomics analysis through LC-ESI-MS/MS on the inflorescences and succulent stems of three ecotypes (saline-alkali land, grassland and sandy land) of *C. deserticola*. A total of 391 common metabolites in six groups were identified, of which isorhamnetin *O*-hexoside (inflorescence) and rosinidin *O*-hexoside (succulent stems) can be used as chemical markers to distinguish succulent stems and inflorescences. Comparing the metabolic differences of three ecotypes, we found that most of the different metabolites related to salt-alkali stress were flavonoids. In particular, we mapped the biosynthetic pathway of phenylethanoid glycosides (PhGs) and showed the metabolic differences in the six groups. To better understand the pharmacodynamic mechanisms and targets of *C. deserticola*, we screened 88 chemical components and 15 potential disease targets through molecular docking. The active ingredients of *C. deserticola* have a remarkable docking effect on the targets of aging diseases such as osteoporosis, vascular disease and atherosclerosis. To explore the use value of inflorescence, we analyzed the molecular docking of the unique flavonoid metabolites in inflorescence with inflammation targets. The results showed that chrysoeriol and cynaroside had higher scores for inflammation targets. This study provides a scientific basis for the discovery and industrialization of the resource value of the non-medicinal parts of *C. deserticola*, and the realization of the sustainable development of *C. deserticola*. It also provides a novel strategy for exploring indications of Chinese herb.

Received 30th May 2021
Accepted 3rd July 2021

DOI: 10.1039/d0ra07488h

rsc.li/rsc-advances

1. Introduction

Cistanche deserticola is an edible and medicinal plant which is often called "desert ginseng".[1] *C. deserticola* was first recorded in Shen Nong's Chinese Materia Medica about 1800 years ago and has been widely used as a traditionally considerable tonic in China and Japan for many years. The compounds that have been isolated from *C. deserticola* are phenylethanoid glycosides (PhGs), iridoids, lignans, fatty acids, alditols, carbohydrates, and polysaccharides, among which PhGs are the main active

[a]*Key Lab of Chinese Medicine Resources Conservation, State Administration of Traditional Chinese Medicine of China, Institute of Medicinal Plant Development, Chinese Academy of Medical Sciences, Peking Union Medical College, Beijing 100193, China. E-mail: 934305103@qq.com*

[b]*Engineering Research Center of Chinese Medicine Resource, Ministry of Education, Beijing 100193, China. E-mail: lfhuang@implad.ac.cn; 15801545922@139.com; Fax: +86-10-62899700; Tel: +86-10-57833197*

[c]*Jiangxi University of Traditional Chinese Medicine, Nanchang 330000, Jiangxi, China*

[d]*Chengdu University of Traditional Chinese Medicine, Chengdu, Sichuan, 611137, China*

[e]*Center for Biotechnology & Microbiology, University of Peshawar, 25000 Peshawar, Pakistan*

† Electronic supplementary information (ESI) available: Table S1: the top 10 differential metabolites of *C. deserticola* by comparison of three habitats groups using VIP (≥1) and fold change (fold change ≥2 or fold change ≤0.5). Table S2: information on potential targets. Table S3: the results of the docking of the main active components in the succulent stems of *C. deserticola* with disease targets. Table S4: the results of the docking of the main active ingredients with the inflammatory target in the inflorescence of *C. deserticola*. Fig. S1: OPLS-DA score map and permutation tests of inflorescence and succulent stem in three ecotypes. Fig. S2: OPLS-DA score map and permutation tests of differential metabolites related to salt-alkali stress. Fig. S3: metabolites of each class content comparison pie chart of inflorescence and succulent stem samples. Fig. S4: predicted binding mode of compounds with targets in three-dimensions (3D). Files S1: metabolome data. See DOI: 10.1039/d0ra07488h

ingredient.[2] Modern pharmacology shows that the extracts of *C. deserticola* (such as phenylethanoid glycosides, polysaccharides, *etc.*) have a wide range of medicinal functions, especially in improving sexual function, enhancing memory, immune regulation, liver protection, laxative activity, antioxidant activity, *etc.*3–5 In addition to its medicinal value, *C. deserticola* has ecological value for desert control due to its ability to grow in arid environments, as well as under saline-alkali stress conditions.[6] However, the wild sources of *C. deserticola* have been considered to be endangered in recent years due to rapidly growing market demand and over-exploitation. It has been listed as one of the class II plants needing protection in China.[2] Consequently, it is urgent to effectively develop *C. deserticola* resources and to determine the best environment for the growth of *C. deserticola*.

Traditional medicinal parts of medicinal plants are widely used, while non-medicinal parts are often discarded. A large number of studies have shown that some non-medicinal parts such as *Salvia miltiorrhiza*, *Paris polyphylla*, and *Crocus sativus* have similar chemical compositions and pharmacological effects to medicinal parts. The research on non-medicinal parts is conducive to the expansion of medicine resources, especially for the protection of endangered medicinal plants.[7,8] Qiao *et al.* used GC-MS technology to identify 40 volatile components in *C. deserticola* inflorescence.[9] Peng *et al.* used transcriptomics and metabolomics to comprehensively analyze the analgesic effects of different parts of citronella.[10] Yang *et al.* isolated five types of flavonoids from the aerial parts of *Salvia miltiorrhiza* and studied their antioxidant activity.[8] The medicinal part of *C. deserticola* is a succulent stem, which causes a large number of inflorescences to be discarded every year, resulting in a huge waste of resources.

Metabolites, as the final products of various biochemical processes catalyzed by enzymes, provide useful molecular insights for the biochemistry of organisms at a given time.[11] Metabolism is closely related to plant quality. Primary metabolites affect plant growth and development, and secondary metabolites can help plants resist environmental stress.[12] Therefore, metabolomics technology is widely used in plant quality evaluation.[13–15] We previously integrated the transcriptome and metabolome to evaluate the quality of the succulent stems of the three ecotypes of *C. deserticola* and explore the molecular mechanism of quality variation.[16] We found that 2′-acetylacteoside can be used as a chemical marker to distinguish three ecotypes. Wenjing Liu *et al.* based on ^{1}H NMR non-targeting to LC-MS-based targeted metabolomics strategy, conducted an in-depth chemical group comparison of four succulent *Cistanche* species and identified echinacoside, acteoside, betaine, mannitol, 6-deoxycatalpol, sucrose, and 8-*epi*-loganic acid can be used as chemical markers to distinguish four *Cistanche* species.[17] Pingping Zou *et al.* applied ^{1}H NMR-based metabolomics to identify the upper and lower parts of *C. deserticola* stem and found that serial primary metabolites, especially carbohydrates and tricarboxylic acid cycle metabolites, as the primary molecules governing the discrimination.[18] HaiLi Qiao *et al.* illustrated that the higher content of esters and aromatics were found in flowers, which were significantly increased in comparison with the volatile compounds from buds through GC-MS analysis of the volatile components of the inflorescence of *C. deserticola*.[9] At present, the research on the quality variation between the succulent stem and inflorescence of *C. deserticola* from the perspective of metabolism is still lacking.

Existing studies have used network simulation of molecular docking to explore the targets and mechanisms of Chinese medicine in treating diseases.[19–21] Jianling Liu *et al.* investigated the effective drug combinations based on system pharmacology among compounds from *Cistanche tubulosa*. They preliminarily screened 61 compounds and 43 targets related to neuroinflammation, of which verbascoside and tubuloside B could play key roles in neuroprotection.[22] YingQi Li *et al.* integrated network pharmacology and zebrafish model to investigate dual-effects components of *Cistanche tubulosa* for treating both osteoporosis and Alzheimer's disease.[23] The chemical components of *C. deserticola* are complex and have a wide range of pharmacological effects. However, therapeutic mechanisms are not yet clear. It is of great significance to clarify disease targets and mechanisms for its further development of *C. deserticola*.

In this study, we used metabolomics to investigate the metabolic differences of the inflorescences and succulent stems of the three ecotypes (saline-alkali land, grassland and sandy land) of *C. deserticola*, and compared the grassland and sandy land ecotypes with the saline-alkali land ecotype to explore the metabolic variation in *C. deserticola* that are affected by salt-alkali stress. Particularly, we identified and analyzed the metabolites of six groups involved in the biosynthesis of PhGs. We applied molecular docking to screen out the potential compounds and targets and drew network simulation diagrams, as well as GO and KEGG enrichment analysis. Our findings provide new insights into the metabolic differences of the inflorescence and succulent stems of the three ecotypes of *C. deserticola*.

2. Materials and methods

2.1 Plant materials and sample collection

We collected the inflorescences (the sample serial number suffix is "1") and succulent stems (the sample serial number suffix is "2") for *C. deserticola* in the excavation stage (April to May 2017) from three different ecotypes: Ebinur Lake of Xinjiang (A1 & A2: saline-alkali land), Tula Village of Xinjiang (B1 & B2: grassland) and Alxa Left Banner of Inner Mongolia (C1 & C2: sandy land) in northwestern China (Table 1 and Fig. 1a). The voucher specimens were deposited in the herbarium of the Institute of Medicinal Plant Development at the Chinese Academy of Medical Sciences in Beijing, China. Samples were collected in the field and stored in liquid nitrogen quickly. After cleaning with PBS, the succulent stem tissues were cut into small pieces and immediately stored at −80 degrees Celsius freezer until further processing. 18 samples (three biological replicates per habitat, two tissue parts per sample) were taken from the thick parts of the inflorescence and fleshy stems for metabolome analysis.

Table 1 List of *Cistanche deserticola* samples used in this study

Sample ID	Sampling site	Ecotypes	Longitude	Latitude	Altitude/m	Tissue	Group
HM1-1	Ebinur Lake, Xinjiang	Saline-alkali land	83.358675	44.881659	211.00	Inflorescence	A1
HM1-2						Succulent stem	A2
HM2-1	Ebinur Lake, Xinjiang	Saline-alkali land	83.152770	44.745758	199.00	Inflorescence	A1
HM2-2						Succulent stem	A2
HM3-1	Ebinur Lake, Xinjiang	Saline-alkali land	83.356425	44.825635	215.43	Inflorescence	A1
HM3-2						Succulent stem	A2
HM4-1	Tula Village, Xinjiang	Grassland	85.540477	46.498027	824.76	Inflorescence	B1
HM4-2						Succulent stem	B2
HM5-1	Tula Village, Xinjiang	Grassland	85.548162	46.493541	797.30	Inflorescence	B1
HM5-2						Succulent stem	B2
HM6-1	Tula Village, Xinjiang	Grassland	85.556225	46.483256	767.32	Inflorescence	B1
HM6-2						Succulent stem	B2
HM26-1	Alxa Left Banner, Inner Mongolia	Sandy land	105.848988	38.834672	2221.87	Inflorescence	C1
HM26-2						Succulent stem	C2
HM27-1	Alxa Left Banner, Inner Mongolia	Sandy land	105.383916	38.828163	1316.97	Inflorescence	C1
HM27-2						Succulent stem	C2
HM28-1	Alxa Left Banner, Inner Mongolia	Sandy land	105.437577	38.725391	1307.60	Inflorescence	C1
HM28-2						Succulent stem	C2

2.2 Extraction and separation of metabolites

The freeze-dried sample was crushed using a mixer mill (MM 400, Retsch) with a zirconia bead for 1.5 min at 30 Hz. 100 mg powder was weighted and extracted overnight at 4 °C with 1.0 mL 70% aqueous methanol. Following centrifugation at 10 000 g for 10 min, the extracts were absorbed (CNWBOND Carbon-GCB SPE Cartridge, 250 mg, 3 mL; ANPEL, Shanghai, China, https://www.anpel.com.cn/cnw) and filtrated (SCAA-104, 0.22 μm pore size; ANPEL, Shanghai, China, http://www.anpel.com.cn/) before LC-MS analysis.

LC-ESI-MS/MS system (UPLC, Shim-pack UFLC SHIMADZU CBM30A system) was used to analyze the lyophilized sample extract. The analytical conditions were as follows: UPLC column, Waters ACQUITY UPLC HSS T3 C18 (1.8 μm, 2.1 mm × 100 mm); solvent, water (0.04% acetic acid): acetonitrile (0.04% acetic acid); gradient program, 100 : 0 v/v at 0 min, 5 : 95 v/v at 11.0 min, 5 : 95 v/v at 12.0 min, 95 : 5 v/v at 12.1 min and 95 : 5 v/v at 15.0 min; flow rate, 0.40 mL min^{-1}; temperature, 40 °C; and injection volume, 2 μL. The effluent was alternatively connected to an ESI-triple quadrupole-linear ion trap (Q TRAP)-MS. In this experiment, a quality control sample was prepared by uniform mixing; during the analysis, quality control samples were run every 10 injections to monitor the stability of the analysis conditions.[24–26]

Linear Ion Trap (LIT) and triple quadrupole (QQQ) scans were acquired on a triple quadrupole-linear ion trap mass spectrometer (Q TRAP), API 6500 Q TRAP LC/MS/MS system, equipped with an ESI turbo ion-spray interface, operating in positive ion mode and controlled by Analyst 1.6 software (AB Sciex). The ESI source operation parameters were as follows: ion source, turbo spray; source temperature 500 °C; ion spray voltage (IS) 5500 V; ion source gas I (GSI), gas II (GSII), curtain gas (CUR) were set at 55, 60, and 25.0 psi, respectively; the collision gas (CAD) was high (12 psi). Instrument tuning and mass calibration were performed with 10 and 100 μmol L^{-1} polypropylene glycol solutions in QQQ and LIT modes, respectively. QQQ scans were acquired as MRM experiments with collision gas (nitrogen) set to 5 psi. Declustering potential (DP) and collision energy (CE) for individual MRM transitions were performed with further optimization. A specific set of MRM transitions was monitored for each period based on the metabolites eluted within this period.

2.3 Metabolite identification and quantification

Qualitative analysis of primary and secondary MS data was carried out by comparison of the precursor ions (Q1), fragment ions (Q3) values (isolation windows (±15 Da), dwell time (ms) or cycle time (1 second)), retention time (RT), and fragmentation patterns with those obtained by injecting standards using the same conditions if the standards were available (Sigma-Aldrich, USA http://www.sigmaaldrich.com/united-states.html) or conducted using a self-compiled database MWDB (MetWare Biological Science and Technology Co., Ltd Wuhan, China) and publicly available metabolite databases if the standards were unavailable. Repeated signals of K^+, Na^+, NH_4^+, and other large molecular weight substances were eliminated during identification. The quantitative analysis of metabolites was based on the MRM mode. The characteristic ions of each metabolite were screened through the QQQ mass spectrometer to obtain the signal strengths. Integration and correction of chromatographic peaks were performed using Multi Quant version 3.0.2 (AB SCIEX, Concord, Ontario, Canada). The corresponding relative metabolite contents were represented as chromatographic peak area integrals.

The VIP (variable important in projection) values of *C. deserticola* samples (three biological replicas) were calculated by SIMCA-P software (version 14.1, Sartorius Stedim Biotech, Umeå, Sweden) based on the principal component analysis and orthogonal partial least squares discriminant analysis. We set fold-change ≥2 or ≤0.5 and VIP value ≥1 as the threshold to

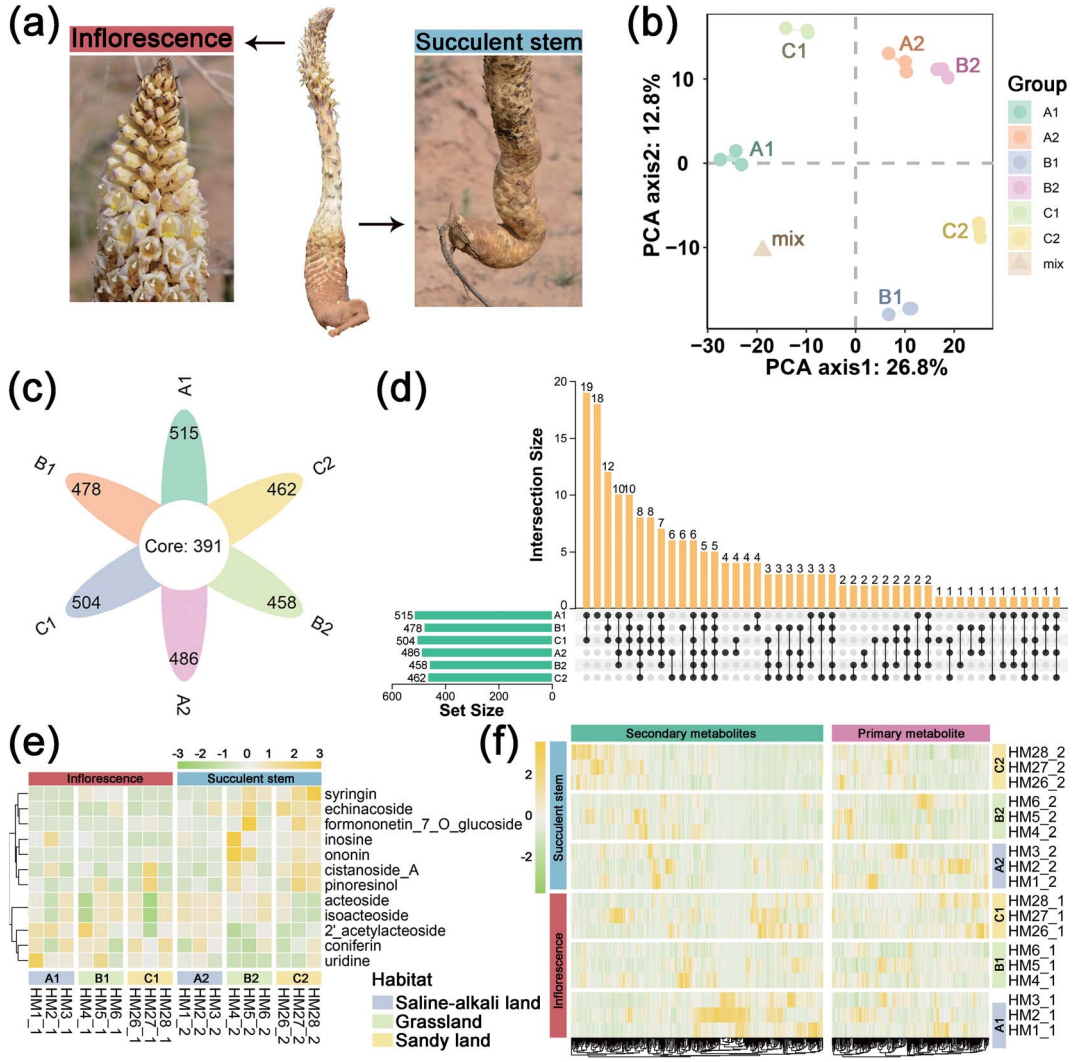

Fig. 1 General metabolite profiles of inflorescence and succulent stem of *Cistanche deserticola* in three ecotypes. (a) A photo of *C. deserticola*, as well as pictures of inflorescence and succulent stem. (b) Principal component analysis of metabolomics data from inflorescence and succulent stem in three ecotypes of the *C. deserticola*. "mix" means the balanced mixture of all samples (quality control). (c) Flower graph showing the number of metabolites in each group and the number of common metabolites. (d) Upset plot showing the similarities and differences of metabolite composition. (e) Heatmap and hierarchical clustering showing the main active ingredients of *C. deserticola* detected by the metabolome. Yellow represents the relatively high content, and the green represents the relatively low content of sample metabolites. (f) Heatmap and hierarchical clustering showing all metabolites, which are divided into primary metabolites and secondary metabolites. Yellow represents relatively high content, and the green represents relatively low content. A1: inflorescence in saline-alkali land, A2: succulent stem in saline-alkali land, B1: inflorescence in grassland, B2: succulent stem in grassland, C1: inflorescence in sandy land, and C2: succulent stem in sandy land.

screen the significantly different metabolites. Metabolite data were normalized, cluster heatmap analysis was performed on all samples and the R program script was used to draw cluster heatmaps.

2.4 Molecular docking

2.4.1 Collection of chemical compounds. Through the preliminary experiment results of our research group and the literature search results, a total of 127 isolated compounds from the succulent stems of *C. deserticola* were collected and downloaded from the Chemical Book website (http://www.chemicalbook.com/) or used ChemDraw to draw the 2D molecular structure. In addition, we found 4 flavonoids (chrysoeriol, cynaroside, hesperetin and homoeriodictyol) detected only in the inflorescence through metabolome results. The 2D structure was converted into a three-dimensional structure with ChemDraw 3D software, and preliminary optimization was performed. Then the preliminary optimized three-dimensional structure was verified by Avogadro software and further energy optimization was used to generate the final compound file format required for subsequent molecular docking.

2.4.2 Collection of target collection. We searched for disease protein targets through literature and the STITCH

database (http://stitch.embl.de/). We obtained the corresponding gene targets by using the Uniport database (http://www.uniport.org/) and retrieved the PDB ID of the protein hypotype and the structure of small molecules by RCSB (http://www.rcsb.org/pdbhome/home.do). When determining the positive drug, we used the literature and the Yaodu website (https://www.pharmacodia.com/cn) to preliminarily identify 45 related disease targets that have been reported, including 10 diseases related to the succulent stems of *C. deserticola* in the literature. These ten diseases were atherosclerosis, osteoporosis, senile dementia, Alzheimer disease, Parkinson, chronic constipation, torsades de pointes ventricular tachycardia, vascular disease, myocardial injury, and rectal cancer. In addition, we collected 467 targets related to inflammation, and obtained 2 important targets (6KBA and 7AWC) through screening, which were used for molecular docking analysis of inflorescence-specific flavonoids.

2.4.3 Molecular docking simulation. To evaluate the binding affinity of compounds in *C. deserticola* to candidate targets, we performed a molecular docking simulation through the software QuickVina 2.0 (https://www.qvina.org), an open-source utility developed by the Alhossary research group. To verify the binding affinity between the targets and the compounds, we calculated a docking score through QuickVina 2.0. The docking scores that exceeded those of the positive drugs (data for every positive drug can be obtained from the corresponding targets in RCSB or literature) indicated a strong binding affinity between candidate targets and the corresponding compounds.[27–30] We used PyMOL (Version 2.0 Schrödinger, LLC) to plot the docking results of the compound and the target.

2.4.4 Component-target-pathway network construction and GO/KEGG function analysis. Component-target-pathway network construction was conducted using the network visualization software Cytoscape (http://cytoscape.org/, 3.7.1). In network interactions, nodes represent components, targets, and pathways, whereas edges represent the interaction of each other. We used the scoring value of molecular docking of the compound and the target gene as an indicator of the color of the connection. The greener the color, the higher the scoring value. A protein–protein interaction (PPI) network associated with gene targets was constructed and analyzed with STRING.[31]

To further find out the biological functions within the constructed network, we used the functional annotation module of the DAVID database[29] to perform Gene Ontology (GO) and KEGG enrichment analyses on target genes.

3. Results

3.1 Metabolic profiles of *C. deserticola*

To obtain an overview of the metabolic changes of the three ecotypes *C. deserticola* inflorescences and succulent stems, widely targeted metabolome analysis was performed using LC-ESI-MS/MS. As shown in Fig. 1b, the inflorescences and succulent stems of *C. deserticola* from different ecotypes showed different separations, and the separation of different tissues was greater than that of different ecotypes. And the three replicate samples have similar PC scores, indicating that *C. deserticola* metabolites showed little separation between replicate samples. Moreover, the quality control (mix) samples clustered together in the center of the PCA scores plot. The petal diagram (Fig. 1c) and upset diagram (Fig. 1d) indicated that there were 391 common metabolites in the six groups, and the number of metabolites detected in the inflorescence was generally higher than that in the succulent stem. The number of metabolites detected in the saline-alkali inflorescence (A1) was the largest, with a total of 515, of which 18 metabolites were only detected in A1. The number of metabolites detected in grassland succulent stems (B2) was the least, with a total of 458, without its unique metabolites.

The relative contents of 578 metabolites were determined, including 35 metabolite categories (ESI File S1†). The most abundant metabolites of the inflorescences and succulent stems in both three ecotypes were lipids, glycerolipids, amino acids, nucleotides and its derivates, phenylethanoid glycosides (PhGs), and flavonoids (Fig. S3a,† 3b and c). After normalization, the proportional content of each metabolite was determined by the average peak response area during UPLC-MS/MS, as shown in Fig. 1e with a heat map, and was further performed with hierarchical clustering analysis. More secondary metabolites showed high relative concentration levels in A1 and C2 than in other groups. Among the secondary metabolites in all three ecotypes, the relative content of phenylethanoid glycosides (PhGs) in the succulent stems was higher than the inflorescences, while the relative content of flavonoids in the inflorescences was higher than the succulent stems.

In this metabolome analysis, 12 main active components of *C. deserticola* were detected, including 2′-acetylacteoside, acteoside, cistanoside A, coniferin, echinacoside, formononetin-7-*O*-glucoside, inosine, isoacteoside, ononin, pinoresinol, syringein, and uridine. A hierarchical clustering heat map (Fig. 1f) was drawn for the main active components of *C. deserticola* detected by the metabolome, showing that the relative content of the main active components in the succulent stem was higher than that in the inflorescence. Compared with different tissues, the active ingredients with relatively high content in inflorescence were 2′-acetylacteoside and coniferin, while the active ingredients with relatively high content in succulent stems were acteoside, cistanoside A, echinacoside, and isoacteoside. Compared with different ecotypes, the relatively high content of active ingredients in saline-alkali land was 2′-acetylacteoside, acteoside, coniferin, echinacoside, and isoacteoside. The relatively high content in grassland was echinacoside, and the relatively high contents in sandy land were cistanoside A.

3.2 Metabolic difference between inflorescence and succulent stem of *C. deserticola*

To understand the difference in metabolism between inflorescence and succulent stem of *C. deserticola* in three ecotypes, we screened the different metabolites. High predictability (Q^2) of the OPLS-DA models was observed to generate a pairwise comparison between inflorescence *versus* Succulent stem in

saline-alkali land ($Q^2 = 0.996$), grassland ($Q^2 = 0.997$), and sandy land ($Q^2 = 0.997$) (Fig. S1a†). The Q^2 and R^2 values were higher in the permutation test than in the OPLS-DA model (Fig. S1b†). To identify potential variables, we set fold-change ≥2 or ≤0.5 and VIP value ≥1 as the threshold to screen the significantly different metabolites in each pair of comparisons. The top 10 different metabolites of the three ecotype inflorescences and succulent stems were shown in Table S1.† Compared with succulent stems, the relatively high content of differential metabolites in inflorescences were flavonoids, such as flavonol, flavone, and flavone *C*-glycosides.

In saline-alkali land, compared with inflorescences, succulent stems had 43 up-regulated differential metabolites and 71 down-regulated differential metabolites (Fig. 2a). The heat map (Fig. 2b) showed that the relative content of the inflorescences was higher than that of the succulent stems. Comparing succulent stems with inflorescences, the main up-regulated metabolites were cyanidin 3-*O*-rutinoside (keracyanin), icariin (kaempferol 3,7-*O*-diglucoside 8-prenyl derivative), homovanillic acid, chlorogenic acid methyl ester, and rosinidin *O*-hexoside. The main down-regulated differential metabolites included *N*′,*N*″-di-*p*-coumaroylspermidine, 8-*C*-hexosyl-luteolin *O*-hexoside, caffeic acid, isorhamnetin *O*-hexoside, and isorhamnetin 5-*O*-hexoside (Fig. 2c). KEGG metabolic pathway enrichment analysis (Fig. 2d) classified the differential metabolites identified from inflorescence and succulent stem into flavonoid biosynthesis, flavone and flavonol biosynthesis, isoflavonoid biosynthesis, phenylpropanoid biosynthesis, and ether lipid metabolism.

In grassland, compared with inflorescences, succulent stems had 35 up-regulated differential metabolites and 54 down-regulated differential metabolites (Fig. 2a). The heat map

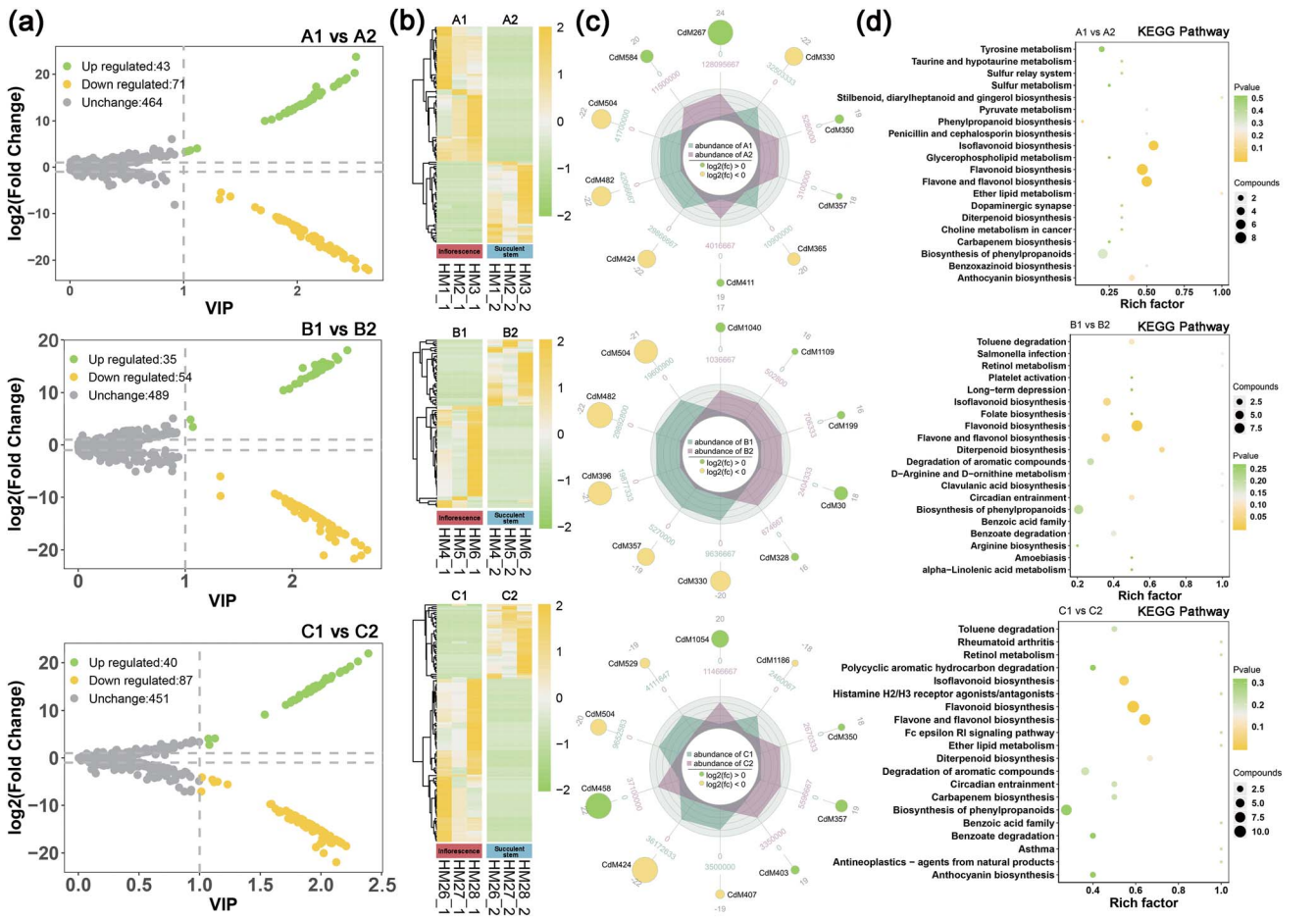

Fig. 2 Differential metabolite profiles of inflorescence and succulent stem of *C. deserticola* in three ecotypes. (a) Volcano map of two issues in three ecotypes; the yellow dots represent downregulated differentially expressed metabolites, the green dots represent upregulated differentially expressed metabolites, and the gray dots represent metabolites detected but not significantly different. (b) Hierarchical clustering analysis for the identification of different metabolites of two tissues in three ecotypes. Yellow represents relatively high content, and the green represents relatively low content. (c) The radar charts showed the top 10 differential metabolites of two tissues in three ecotypes. The number in the middle of each branch is the relative content, and the number in each circle is the $\log_2$ fold change value. (d) KEGG pathway enrichment results of differential metabolites of two tissues in three ecotypes. The rich factor is the ratio of the number of differentially expressed metabolites in the pathway to the total number of metabolites annotated by the pathway. The larger the value, the greater the degree of enrichment. The closer the *p*-value is to 0, the more significant the enrichment. The size of the dot in the figure represents the number of significantly different metabolites enriched in the corresponding pathway. A1: inflorescence in saline-alkali land, A2: succulent stem in saline-alkali land, B1: inflorescence in grassland, B2: succulent stem in grassland, C1: inflorescence in sandy land, and C2: succulent stem in sandy land.

(Fig. 2b) showed that the relative content of the inflorescences was higher than that of the succulent stems. Comparing succulent stems with inflorescences, the main up-regulated metabolites were L-(+)-arginine, adipic acid, *N*-methylnicotinamide, 4-hydroxybenzoic acid, and dihydromyricetin. The main down-regulated differential metabolites included rosinidin *O*-hexoside, caffeic acid, isorhamnetin *O*-hexoside, selgin 5-*O*-hexoside, and isorhamnetin 5-*O*-hexoside (Fig. 2c). KEGG metabolic pathway enrichment analysis (Fig. 2d) classified the differential metabolites identified from inflorescence and succulent stem into flavonoid biosynthesis, flavone and flavonol biosynthesis, diterpenoid biosynthesis, isoflavonoid biosynthesis, and circadian entrainment.

In sandy land, compared with inflorescences, succulent stems had 40 up-regulated differential metabolites and 87 down-regulated differential metabolites (Fig. 2a). The heat map (Fig. 2b) showed that the relative content of the inflorescences was higher than that of the succulent stems. Comparing succulent stems with inflorescences, the main up-regulated metabolites were *O*-feruloyl 4-hydroxylcoumarin, syringing, rosinidin *O*-hexoside, 3-(4-hydroxyphenyl) propionic acid, and homovanillic acid. The main down-regulated differential metabolites included chrysoeriol *O*-rhamnosyl-*O*-glucuronic acid, *C*-hexosyl-apigenin *O*-caffeoylhexoside, selgin *O*-malonylhexoside, isorhamnetin *O*-hexoside, and 8-*C*-hexosyl-luteolin *O*-hexoside (Fig. 2c). KEGG metabolic pathway enrichment analysis (Fig. 2d) classified the differential metabolites identified from inflorescence and succulent stem into flavone and flavonol biosynthesis, flavonoid biosynthesis, isoflavonoid biosynthesis, diterpenoid biosynthesis, and degradation of aromatic compounds.

3.3 Metabolic differences related to saline-alkali stress in three ecotypes of *C. deserticola*

In order to grasp the unique metabolic characteristics of the three ecotypes of the saline-alkali land of *C. deserticola*, we screened the different metabolites in saline-alkali land *versus* grassland and sandy land *versus* saline-alkali land. High predictability (Q^2) of the OPLS-DA models was observed to generate a pairwise comparison between saline-alkali land *versus* grassland of inflorescence ($Q^2 = 0.997$) and succulent stem ($Q^2 = 0.991$). Meanwhile, high predictability (Q^2) of the OPLS-DA models between sandy land *versus* saline-alkali land of inflorescence ($Q^2 = 0.988$) and succulent stem ($Q^2 = 0.995$). The Q^2 and R^2 values were higher in the permutation test than in the OPLS-DA model (Fig. S2†). To identify potential variables, we set fold-change ≥ 2 or ≤ 0.5 and VIP value ≥ 1 as the threshold to screen the significantly different metabolites in each pair of comparisons. Table 2 showed the different metabolites of inflorescences and succulent stems related to saline-alkali stress (saline-alkali land *vs.* grassland and sandy land *vs.* saline-alkali land), sorted by metabolite category, and demonstrated that the most metabolites class was flavonoid. Among them, the relative content of anthocyanins, flavonoid, flavonol, flavanone, catechin and their derivatives, and isoflavone are the highest in saline-alkali land. Furthermore, the heatmap (Fig. 3d) showed that the groups with higher relative content of differential metabolites of flavonoids were A1 and C1. The relative content of anthocyanins was the highest in the A2 group, and the relative content of flavonoids and flavonols was the highest in the A1 group.

The volcano maps (Fig. 3a) showed that the number of up-regulated differential metabolism in saline-alkali soils is higher than that of grassland and sandy soils, whether in inflorescences or succulent stems. The top 20 differential metabolites of each comparison were shown in Fig. 3b. In saline-alkali land *vs.* grassland, the KEGG pathways of differential metabolites of inflorescence were mainly enriched in flavonoid biosynthesis, flavonol, and flavonol biosynthesis, diterpenoid biosynthesis, isoflavonoid biosynthesis, and biosynthesis of phenylpropanoids. Besides, the KEGG pathways of the different metabolites of the succulent stem were mainly enriched in the dopaminergic synapse, purine metabolism, flavonoid biosynthesis, pyrimidine metabolism, and circadian entrainment. In saline-alkali land *vs.* grassland, the KEGG pathways of differential metabolites of inflorescence were mainly enriched in isoflavonoid biosynthesis, biosynthesis of secondary metabolites, flavone and flavonol biosynthesis, antineoplastics-agents from natural products, and asthma. Moreover, the KEGG pathways of the different metabolites of the succulent stem were mainly enriched in aminoacyl-tRNA biosynthesis, protein digestion and absorption, central carbon metabolism in cancer, biosynthesis of amino acids, and biosynthesis of phenylpropanoids (Fig. 3c).

3.4 Mapping of differential metabolites related to phenylethanoid glycosides (PhGs) biosynthesis pathway

Previously, we have integrated transcriptomic and metabolomic analysis to explore the biosynthetic pathways of PhGs in the succulent stems of *C. deserticola*.[16] To discover the molecular mechanism leading to the difference in metabolism between inflorescence and succulent stem, we reconstructed the biosynthetic pathway of PhGs (Fig. 4). It mainly contained four KEGG pathways: "phenylpropanoid biosynthesis (Ko00940)", "phenylalanine, tyrosine and tryptophan biosynthesis (Ko00400)", "tyrosine metabolism (Ko00350)" and "phenylalanine metabolism (Ko00360)". The results in Fig. 4 showed that the relative content of compounds in the PhGs biosynthesis pathway varied with the tissues (inflorescences and succulent stems) and ecotypes (saline-alkali land, grassland, and sandy land) of *C. deserticola*. In grassland ecotype, the relative contents of tyrosine and cinnamic acid were up-regulated in succulent stems. Both in saline-alkali land and grassland ecotype, the relative contents of caffeic acid were up-regulated in inflorescences. Metabolome analysis detected three phenylethanoid glycosides (PhGs), namely isoacteoside, acteoside, and 2′-acetylacteoside, and their relative content was the highest in the A2 group.

3.5 Molecular docking analysis of the main active components of *C. deserticola*

The collected 45 related disease targets were molecularly docked with 127 compounds of *C. deserticola*. Based on the

Table 2 Differential metabolites and their classes related to salt-alkali stress of *C. deserticola*[a]

		Saline-alkali land *vs.* grassland						Sandy land *vs.* saline-alkali land						
		Inflorescence (A1 *vs.* B1)			Succulent stem (A2 *vs.* B2)			Inflorescence (C1 *vs.* A1)			Succulent stem (C2 *vs.* A2)			
No.	Compounds	VIP	Fold change	Type	VIP	Fold change	Type	VIP	Fold change	Type	VIP	Fold change	Type	Class
CdM781	1-Methylhistidine	2.01×10^{0}	1.86×10^{-4}	Down	—	—	—	—	—	—	—	—	—	Amino acid d
CdM182	L-Methionine methyl ester	2.11×10^{0}	7.96×10^{-5}	Down	2.44×10^{0}	2.12×10^{4}	Up	—	—	—	—	—	—	erivatives
CdM1039	2,3-Dimethylsuccinic acid	2.40×10^{0}	5.03×10^{-6}	Down	—	—	—	—	—	—	—	—	—	
CdM1064	Pyrrole-2-carboxylic acid	—	—	—	2.23×10^{0}	1.93×10^{-4}	Down	—	—	—	2.13×10^{0}	5.18×10^{3}	Up	
CdM781	1-Methylhistidine	—	—	—	2.39×10^{0}	1.95×10^{4}	Up	—	—	—	—	—	—	
CdM192	3-Chloro-L-tyrosine	—	—	—	2.40×10^{0}	7.71×10^{-5}	Down	2.67×10^{0}	5.12×10^{-5}	Down	2.29×10^{0}	1.30×10^{4}	Up	
CdM371	*N*-Phenylacetylglycine	—	—	—	2.50×10^{0}	4.44×10^{4}	Up	—	—	—	2.41×10^{0}	2.64×10^{-5}	Down	
CdM19	3-*N*-Methyl-L-histidine	—	—	—	2.65×10^{0}	1.72×10^{5}	Up	—	—	—	—	—	—	
CdM393	Phe–Phe	—	—	—	—	—	—	2.51×10^{0}	1.61×10^{-4}	Down	2.13×10^{0}	2.84×10^{-4}	Down	
CdM11	Histamine	—	—	—	—	—	—	—	—	—	2.28×10^{0}	1.92×10^{4}	Up	
CdM799	L-Citrulline	2.15×10^{0}	5.08×10^{-5}	Down	—	—	—	—	—	—	—	—	—	Amino acids
CdM30	L-(+)-Arginine	2.25×10^{0}	1.26×10^{-5}	Down	—	—	—	—	—	—	—	—	—	
CdM837	L-Cysteine	—	—	—	—	—	—	2.58×10^{0}	3.18×10^{4}	Up	2.32×10^{0}	4.51×10^{-5}	Down	
CdM1087	Cyanidin *O*-diacetyl-hexoside-*O*-glyceric acid	1.84×10^{0}	1.54×10^{3}	Up	2.36×10^{0}	9.79×10^{-5}	Down	—	—	—	—	—	—	Anthocyanins
CdM317	Peonidin *O*-hexoside	2.17×10^{0}	2.11×10^{4}	Up	—	—	—	—	—	—	—	—	—	
CdM230	Delphinidin 3-*O*-glucoside (mirtillin)	2.21×10^{0}	3.32×10^{-5}	Down	2.45×10^{0}	1.94×10^{4}	Up	—	—	—	—	—	—	
CdM357	Rosinidin *O*-hexoside	2.51×10^{0}	5.86×10^{5}	Up	2.76×10^{0}	2.90×10^{-6}	Down	—	—	—	—	—	—	
CdM267	Cyanidin 3-*O*-rutinoside (keracyanin)	—	—	—	2.92×10^{0}	7.03×10^{-8}	Down	—	—	—	2.80×10^{0}	1.42×10^{7}	Up	
CdM270	Petunidin 3-*O*-glucoside	—	—	—	—	—	—	2.72×10^{0}	2.63×10^{4}	Up	—	—	—	
CdM255	Syringic acid *O*-feruloyl-*O*-hexoside	2.25×10^{0}	4.43×10^{4}	Up	—	—	—	—	—	—	2.38×10^{0}	2.64×10^{-5}	Down	Benzoic acid
CdM1059	2,4-Dihydroxybenzoic acid	2.47×10^{0}	2.20×10^{-6}	Down	—	—	—	—	—	—	—	—	—	derivatives
CdM733	4-Hydroxy-3,5-diisopropylbenzaldehyde	—	—	—	1.04×10^{0}	2.11×10^{-2}	Down	—	—	—	2.41×10^{0}	1.64×10^{5}	Up	
CdM989	Gallic acid *O*-hexoside	—	—	—	2.14×10^{0}	5.14×10^{-4}	Down	—	—	—	2.05×10^{0}	1.94×10^{3}	Up	
CdM630	3,4-Dihydrocoumarin	2.00×10^{0}	2.08×10^{-4}	Down	2.30×10^{0}	1.58×10^{-4}	Down	—	—	—	2.20×10^{0}	6.32×10^{3}	Up	Coumarins
CdM528	6-Hydroxy-4-methylcoumarin	2.11×10^{0}	1.29×10^{4}	Up	2.42×10^{0}	2.28×10^{4}	Up	—	—	—	2.43×10^{0}	2.14×10^{-5}	Down	
CdM241	*O*-Feruloyl coumarin	2.11×10^{0}	1.21×10^{4}	Up	—	—	—	3.05×10^{0}	8.07×10^{5}	Up	2.27×10^{0}	7.67×10^{-5}	Down	
CdM359	Daphnetin	2.24×10^{0}	4.28×10^{4}	Up	1.06×10^{0}	1.43×10^{1}	Up	2.84×10^{0}	1.08×10^{-5}	Down	1.07×10^{0}	1.16×10^{-1}	Down	
CdM426	*N*-Sinapoyl hydroxycoumarin	2.36×10^{0}	1.27×10^{5}	Up	2.57×10^{0}	1.35×10^{-5}	Down	—	—	—	2.46×10^{0}	7.40×10^{4}	Up	
CdM1086	Esculetin (6,7-dihydroxycoumarin)	—	—	—	1.25×10^{0}	9.05×10^{-2}	Down	—	—	—	1.03×10^{0}	6.69×10^{0}	Up	
CdM495	Hesperetin 7-*O*-neohesperidoside (neohesperidin)	2.07×10^{0}	8.68×10^{-5}	Down	—	—	—	—	—	—	—	—	—	Flavanone
CdM603	Eriodictyol	2.16×10^{0}	4.80×10^{-5}	Down	—	—	—	—	—	—	2.28×10^{0}	2.46×10^{4}	Up	
CdM464		2.41×10^{0}	4.92×10^{-6}	Down	—	—	—	—	—	—	2.54×10^{0}	2.51×10^{5}	Up	

Table 2 (*Contd.*)

		Saline-alkali land *vs.* grassland						Sandy land *vs.* saline-alkali land						
		Inflorescence (A1 *vs.* B1)			Succulent stem (A2 *vs.* B2)			Inflorescence (C1 *vs.* A1)			Succulent stem (C2 *vs.* A2)			
No.	Compounds	VIP	Fold change	Type	VIP	Fold change	Type	VIP	Fold change	Type	VIP	Fold change	Type	Class
	Naringenin 7-*O*-neohesperidoside (naringin)													
CdM1148	Hesperetin 5-*O*-glucoside	2.48×10^{0}	1.22×10^{-6}	Down	—	—	—	3.08×10^{0}	8.20×10^{5}	Up	—	—	—	
CdM731	Xanthohumol	—	—	—	2.06×10^{0}	7.96×10^{-4}	Down	—	—	—	—	—	—	
CdM1203	Naringenin 7-*O*-glucoside (prunin)	—	—	—	2.42×10^{0}	4.95×10^{-5}	Down	—	—	—	2.31×10^{0}	2.02×10^{4}	Up	
CdM1024	Chrysoeriol *O*-hexosyl-*O*-malonylhexoside	1.74×10^{0}	6.41×10^{2}	Up	2.19×10^{0}	3.04×10^{-4}	Down	—	—	—	—	—	—	Flavone
CdM1202	Tricin 7-*O*-hexoside	1.90×10^{0}	3.45×10^{-4}	Down	—	—	—	—	—	—	—	—	—	
CdM553	Tricin *O*-malonylhexoside	1.94×10^{0}	3.35×10^{-4}	Down	2.40×10^{0}	4.16×10^{-5}	Down	—	—	—	—	—	—	
CdM506	Chrysoeriol *O*-hexosyl-*O*-hexoside	1.94×10^{0}	2.97×10^{-4}	Down	2.06×10^{0}	1.35×10^{3}	Up	—	—	—	—	—	—	
CdM1193	Tricin *O*-glucuronic acid	2.01×10^{0}	5.27×10^{3}	Up	—	—	—	—	—	—	2.21×10^{0}	1.44×10^{-4}	Down	
CdM1326	Acacetin	2.06×10^{0}	6.54×10^{-5}	Down	—	—	—	—	—	—	—	—	—	
CdM503	Syringetin 7-*O*-hexoside	2.10×10^{0}	6.86×10^{-5}	Down	2.74×10^{0}	4.15×10^{-6}	Down	—	—	—	2.62×10^{0}	2.41×10^{5}	Up	
CdM381	Limocitrin *O*-hexoside	2.12×10^{0}	1.47×10^{4}	Up	2.44×10^{0}	1.89×10^{4}	Up	—	—	—	—	—	—	
CdM353	Chrysoeriol *O*-glucuronic acid-*O*-hexoside	2.13×10^{0}	6.53×10^{-5}	Down	2.31×10^{0}	1.52×10^{-4}	Down	—	—	—	2.21×10^{0}	6.57×10^{3}	Up	
CdM434	Acacetin *O*-glucuronic acid	2.25×10^{0}	1.50×10^{-5}	Down	—	—	—	—	—	—	2.40×10^{0}	1.15×10^{5}	Up	
CdM510	Apigenin 7-*O*-glucoside (cosmosiin)	2.37×10^{0}	4.97×10^{-6}	Down	—	—	—	—	—	—	2.39×10^{0}	4.41×10^{4}	Up	
CdM1253	Luteolin	2.38×10^{0}	2.54×10^{-6}	Down	—	—	—	1.49×10^{0}	4.59×10^{1}	Up	—	—	—	
CdM529	Selgin *O*-malonylhexoside	2.63×10^{0}	4.57×10^{-7}	Down	2.47×10^{0}	3.67×10^{-5}	Down	1.25×10^{0}	4.79×10^{0}	Up	2.36×10^{0}	2.72×10^{4}	Up	
CdM492	Chrysoeriol 7-*O*-rutinoside	—	—	—	2.29×10^{0}	1.62×10^{-4}	Down	—	—	—	2.19×10^{0}	6.18×10^{3}	Up	
CdM515	Chrysoeriol *O*-glucuronic acid	—	—	—	2.34×10^{0}	3.67×10^{-5}	Down	—	—	—	2.24×10^{0}	2.72×10^{4}	Up	
CdM595	Chrysin *O*-hexoside	—	—	—	2.35×10^{0}	1.03×10^{-4}	Down	—	—	—	2.25×10^{0}	9.68×10^{3}	Up	
CdM594	Chrysin 5-*O*-glucoside (toringin)	—	—	—	2.36×10^{0}	8.14×10^{-5}	Down	—	—	—	2.26×10^{0}	1.23×10^{4}	Up	
CdM543	Apigenin *O*-malonylhexoside	—	—	—	2.37×10^{0}	9.35×10^{-5}	Down	—	—	—	2.27×10^{0}	1.07×10^{4}	Up	
CdM1186	Chrysoeriol *O*-rhamnosyl-*O*-glucuronic acid	—	—	—	2.45×10^{0}	1.11×10^{-5}	Down	—	—	—	2.35×10^{0}	9.03×10^{4}	Up	
CdM396	Selgin 5-*O*-hexoside	—	—	—	2.47×10^{0}	3.13×10^{-5}	Down	—	—	—	—	—	—	
CdM485	Syringetin 5-*O*-hexoside	—	—	—	2.74×10^{0}	3.93×10^{-6}	Down	2.85×10^{0}	9.84×10^{-6}	Down	2.62×10^{0}	2.54×10^{5}	Up	
CdM1202	Tricin 7-*O*-hexoside	—	—	—	—	—	—	2.36×10^{0}	2.90×10^{3}	Up	—	—	—	
CdM553	Tricin *O*-malonylhexoside	—	—	—	—	—	—	2.41×10^{0}	2.99×10^{3}	Up	2.29×10^{0}	2.41×10^{4}	Up	
CdM506	Chrysoeriol *O*-hexosyl-*O*-hexoside	—	—	—	—	—	—	2.41×10^{0}	3.36×10^{3}	Up	—	—	—	
CdM522	Spinacetin	—	—	—	—	—	—	2.48×10^{0}	1.20×10^{-4}	Down	—	—	—	
CdM1030	Luteolin *O*-hexosyl-*O*-hexosyl-*O*-hexoside	—	—	—	—	—	—	2.48×10^{0}	5.75×10^{3}	Up	—	—	—	
CdM556	Chrysoeriol *O*-malonylhexoside	—	—	—	—	—	—	2.62×10^{0}	7.15×10^{-5}	Down	2.30×10^{0}	5.96×10^{-5}	Down	

Table 2 (*Contd.*)

		Saline-alkali land *vs.* grassland						Sandy land *vs.* saline-alkali land						
		Inflorescence (A1 *vs.* B1)			Succulent stem (A2 *vs.* B2)			Inflorescence (C1 *vs.* A1)			Succulent stem (C2 *vs.* A2)			
No.	Compounds	VIP	Fold change	Type	VIP	Fold change	Type	VIP	Fold change	Type	VIP	Fold change	Type	Class
CdM1135	Tricin *O*-saccharic acid	—	—	—	—	—	—	—	—	—	1.03×10^{0}	1.43×10^{-1}	Down	
CdM1211	Baicalein-7-*O*-glucuronide (baicalin)	—	—	—	—	—	—	—	—	—	1.36×10^{0}	3.56×10^{2}	Up	
CdM379	Tricin 7-*O*-hexosyl-*O*-hexoside	—	—	—	—	—	—	—	—	—	2.26×10^{0}	1.05×10^{4}	Up	
CdM555	Tricetin *O*-malonylhexoside	—	—	—	—	—	—	—	—	—	2.40×10^{0}	4.16×10^{-5}	Down	
CdM632	Apigenin	—	—	—	—	—	—	—	—	—	2.36×10^{0}	4.82×10^{4}	Up	
CdM471	Apigenin 7-rutinoside (isorhoifolin)	—	—	—	—	—	—	—	—	—	2.36×10^{0}	1.42×10^{5}	Up	
CdM342	Tricin 5-*O*-hexosyl-*O*-hexoside	—	—	—	—	—	—	—	—	—	2.37×10^{0}	2.59×10^{4}	Up	
CdM490	Apigenin 7-*O*-neohesperidoside (rhoifolin)	—	—	—	—	—	—	—	—	—	2.52×10^{0}	1.84×10^{5}	Up	
CdM525	Apigenin 8-*C*-pentoside	2.06×10^{0}	8.40×10^{3}	Up	—	—	—	2.62×10^{0}	4.52×10^{-5}	Down	—	—	—	Flavone
CdM370	8-*C*-Hexosyl-luteolin *O*-pentoside	2.15×10^{0}	1.70×10^{4}	Up	—	—	—	2.69×10^{0}	3.80×10^{-5}	Down	—	—	—	*C*-glycosides
CdM1096	Eriodictyol *C*-hexoside	2.22×10^{0}	1.04×10^{-5}	Down	2.45×10^{0}	2.36×10^{-5}	Down	—	—	—	2.35×10^{0}	4.25×10^{4}	Up	
CdM345	*C*-Hexosyl-apigenin *O*-feruloylhexoside-*O*-hexoside	2.26×10^{0}	1.95×10^{-5}	Down	—	—	—	2.81×10^{0}	5.12×10^{4}	Up	—	—	—	
CdM286	8-*C*-Hexosyl-hesperetin *O*-hexoside	2.32×10^{0}	6.94×10^{-6}	Down	—	—	—	2.88×10^{0}	1.44×10^{5}	Up	—	—	—	
CdM498	*C*-Pentosyl-apigenin *O*-*p*-coumaroylhexoside	2.35×10^{0}	1.26×10^{5}	Up	2.54×10^{0}	1.97×10^{-5}	Down	2.90×10^{0}	9.61×10^{-6}	Down	1.10×10^{0}	1.17×10^{1}	Up	
CdM288	Chrysoeriol 6-*C*-hexoside 8-*C*-hexoside-*O*-hexoside	2.37×10^{0}	1.47×10^{5}	Up	—	—	—	—	—	—	2.32×10^{0}	5.87×10^{-5}	Down	
CdM424	8-*C*-Hexosyl-luteolin *O*-hexoside	2.67×10^{0}	3.01×10^{-7}	Down	—	—	—	—	—	—	—	—	—	
CdM366	6-*C*-Hexosyl-hesperetin *O*-hexoside	—	—	—	2.51×10^{0}	3.83×10^{4}	Up	—	—	—	—	—	—	
CdM373	*C*-Hexosyl-chrysoeriol *O*-rutinoside	—	—	—	—	—	—	2.61×10^{0}	1.31×10^{4}	Up	—	—	—	
CdM386	*C*-Hexosyl-chrysoeriol *O*-hexoside	—	—	—	—	—	—	2.72×10^{0}	3.93×10^{-5}	Down	2.36×10^{0}	3.28×10^{4}	Up	
CdM504	Isorhamnetin *O*-hexoside	1.19×10^{0}	4.70×10^{-1}	Down	—	—	—	1.24×10^{0}	4.32×10^{0}	Up	—	—	—	Flavonol
CdM1297	Isorhamnetin	1.89×10^{0}	5.43×10^{-4}	Down	—	—	—	2.34×10^{0}	1.84×10^{3}	Up	—	—	—	
CdM670	3,7-Di-*O*-methylquercetin	1.97×10^{0}	2.73×10^{-4}	Down	—	—	—	—	—	—	—	—	—	
CdM398	Isorhamnetin 3-*O*-neohesperidoside	2.01×10^{0}	1.86×10^{-4}	Down	—	—	—	—	—	—	2.09×10^{0}	2.69×10^{3}	Up	
CdM474	Kaempferide	2.01×10^{0}	6.30×10^{3}	Up	—	—	—	—	—	—	—	—	—	
CdM1189	Dihydroquercetin (taxifolin)	2.02×10^{0}	8.04×10^{-5}	Down	—	—	—	—	—	—	—	—	—	
CdM1230	Aromadedrin (dihydrokaempferol)	2.06×10^{0}	9.40×10^{-5}	Down	—	—	—	—	—	—	—	—	—	
CdM1143		2.08×10^{0}	9.25×10^{-5}	Down	—	—	—	2.58×10^{0}	1.08×10^{4}	Up	—	—	—	

Table 2 (*Contd.*)

		Saline-alkali land *vs.* grassland						Sandy land *vs.* saline-alkali land						
		Inflorescence (A1 *vs.* B1)			Succulent stem (A2 *vs.* B2)			Inflorescence (C1 *vs.* A1)			Succulent stem (C2 *vs.* A2)			
No.	Compounds	VIP	Fold change	Type	VIP	Fold change	Type	VIP	Fold change	Type	VIP	Fold change	Type	Class
	Kaempferol 3-*O*-rutinoside (nicotiflorin)													
CdM1123	Kaempferol 3-*O*-robinobioside (biorobin)	2.10×10^{0}	8.40×10^{-5}	Down	—	—	—	—	—	—	—	—	—	
CdM308	Quercetin 5-*O*-malonylhexosyl-hexoside	2.22×10^{0}	1.95×10^{-5}	Down	—	—	—	2.76×10^{0}	5.12×10^{4}	Up	—	—	—	
CdM1164	Quercetin *O*-acetylhexoside	2.34×10^{0}	4.23×10^{-6}	Down	—	—	—	2.91×10^{0}	2.37×10^{5}	Up	—	—	—	
CdM1149	Quercetin 3-*O*-glucoside (isotrifoliin)	2.47×10^{0}	1.24×10^{-6}	Down	—	—	—	3.07×10^{0}	8.08×10^{5}	Up	—	—	—	
CdM1206	Isorhamnetin *O*-acetyl-hexoside	2.51×10^{0}	1.45×10^{-6}	Down	2.12×10^{0}	5.77×10^{-4}	Down	3.12×10^{0}	6.92×10^{5}	Up	2.03×10^{0}	1.73×10^{3}	Up	
CdM457	Methyl quercetin *O*-hexoside	2.54×10^{0}	1.19×10^{-6}	Down	—	—	—	3.15×10^{0}	8.42×10^{5}	Up	—	—	—	
CdM1298	Di-*O*-methylquercetin	—	—	—	1.17×10^{0}	7.35×10^{-2}	Down	—	—	—	1.08×10^{0}	1.16×10^{1}	Up	
CdM466	Kaempferol 3-*O*-galactoside (trifolin)	—	—	—	2.42×10^{0}	1.78×10^{4}	Up	—	—	—	2.50×10^{0}	1.23×10^{-5}	Down	
CdM460	Quercetin 4′-*O*-glucoside (spiraeoside)	—	—	—	2.42×10^{0}	5.47×10^{-5}	Down	3.18×10^{0}	2.24×10^{6}	Up	2.32×10^{0}	1.83×10^{4}	Up	
CdM584	Icariin (kaempferol 3, 7-*O*-diglucoside 8-prenyl derivative)	—	—	—	2.91×10^{0}	7.83×10^{-7}	Down	—	—	—	1.39×10^{0}	3.60×10^{1}	Up	
CdM497	Kaempferol 3-*O*-glucoside (astragalin)	—	—	—	—	—	—	2.51×10^{0}	9.11×10^{3}	Up	—	—	—	
CdM1109	Dihydromyricetin	—	—	—	—	—	—	2.66×10^{0}	3.65×10^{-5}	Down	—	—	—	
CdM482	Isorhamnetin 5-*O*-hexoside	—	—	—	—	—	—	3.34×10^{0}	4.67×10^{6}	Up	—	—	—	
CdM341	6-Hydroxymethylherniarin	1.95×10^{0}	3.40×10^{3}	Up	2.35×10^{0}	9.38×10^{-5}	Down	2.58×10^{0}	9.90×10^{-5}	Down	—	—	—	Hydroxycin-namoyl derivatives
CdM433	Sinapic acid	2.06×10^{0}	1.26×10^{-4}	Down	—	—	—	—	—	—	—	—	—	
CdM508	*p*-Coumaraldehyde	2.36×10^{0}	1.22×10^{5}	Up	2.63×10^{0}	1.36×10^{5}	Up	—	—	—	—	—	—	
CdM403	3-(4-Hydroxyphenyl)propionic acid	2.49×10^{0}	4.63×10^{5}	Up	2.73×10^{0}	2.90×10^{5}	Up	—	—	—	2.67×10^{0}	2.69×10^{-6}	Down	
CdM1054	Syringin	2.49×10^{0}	5.06×10^{5}	Up	—	—	—	—	—	—	1.05×10^{0}	1.31×10^{-1}	Down	
CdM1248	3,4,5-Trimethoxycinnamic acid	—	—	—	1.01×10^{0}	2.08×10^{-2}	Down	—	—	—	—	—	—	
CdM1271	4-Methoxycinnamic acid	—	—	—	1.09×10^{0}	8.21×10^{-2}	Down	—	—	—	—	—	—	
CdM1273	3,4-Dimethoxycinnamic acid	—	—	—	1.26×10^{0}	3.43×10^{-2}	Down	—	—	—	—	—	—	
CdM295	Gallic acid *O*-feruloyl-*O*-hexosyl-*O*-hexoside	—	—	—	2.43×10^{0}	5.88×10^{-5}	Down	2.64×10^{0}	6.91×10^{-5}	Down	—	—	—	
CdM1080	1-*O*-Beta-D-glucopyranosyl sinapate	—	—	—	2.44×10^{0}	4.25×10^{-5}	Down	—	—	—	2.34×10^{0}	2.35×10^{4}	Up	
CdM508	*p*-Coumaraldehyde	—	—	—	—	—	—	—	—	—	2.61×10^{0}	4.17×10^{-6}	Down	
CdM403	3-(4-Hydroxyphenyl)propionic acid	—	—	—	—	—	—	—	—	—	—	—	—	
CdM350	Homovanillic acid	—	—	—	2.83×10^{0}	1.70×10^{-6}	Down	—	—	—	—	—	—	

Table 2 (*Contd.*)

		Saline-alkali land *vs.* grassland						Sandy land *vs.* saline-alkali land						
		Inflorescence (A1 *vs.* B1)			Succulent stem (A2 *vs.* B2)			Inflorescence (C1 *vs.* A1)			Succulent stem (C2 *vs.* A2)			
No.	Compounds	VIP	Fold change	Type	VIP	Fold change	Type	VIP	Fold change	Type	VIP	Fold change	Type	Class
CdM330	Caffeic acid	—	—	—	—	—	—	3.20×10^{0}	3.61×10^{6}	Up	2.53×10^{0}	6.55×10^{-6}	Down	
CdM1158	Coniferyl alcohol	—	—	—	—	—	—	—	—	—	2.19×10^{0}	5.48×10^{3}	Up	
CdM1209	6-Hydroxydaidzein	2.04×10^{0}	9.00×10^{-5}	Down	—	—	—	—	—	—	—	—	—	Isoflavone
CdM1325	Prunetin	2.06×10^{0}	6.26×10^{-5}	Down	—	—	—	—	—	—	—	—	—	
CdM583	Orobol (5,7,3′,4′-tetrahydroxyisoflavone)	2.16×10^{0}	2.56×10^{-5}	Down	—	—	—	2.68×10^{0}	3.91×10^{4}	Up	—	—	—	
CdM1213	2′-Hydroxydaidzein	2.19×10^{0}	3.31×10^{-5}	Down	—	—	—	—	—	—	—	—	—	
CdM623	Genistein (4′,5,7-trihydroxyisoflavone)	2.23×10^{0}	1.99×10^{-5}	Down	—	—	—	2.77×10^{0}	5.02×10^{4}	Up	—	—	—	
CdM465	Genistein 7-*O*-glucoside (genistin)	2.38×10^{0}	4.59×10^{-6}	Down	—	—	—	—	—	—	2.42×10^{0}	5.27×10^{4}	Up	
CdM1226	Formononetin 7-*O*-glucoside (ononin)	—	—	—	—	—	—	2.41×10^{0}	3.23×10^{-4}	Down	—	—	—	
CdM579	2′-Hydroxygenistein	—	—	—	—	—	—	2.92×10^{0}	2.08×10^{5}	Up	—	—	—	
CdM1115	Glycitin	—	—	—	—	—	—	—	—	—	2.27×10^{0}	8.80×10^{-5}	Down	
CdM678	MAG (18 : 4) isomer 1	2.21×10^{0}	1.94×10^{-5}	Down	2.52×10^{0}	1.78×10^{-5}	Down	—	—	—	2.41×10^{0}	5.62×10^{4}	Up	Lipids
CdM712	MAG (18 : 3) isomer 5	—	—	—	1.03×10^{0}	6.84×10^{-2}	Down	—	—	—	—	—	—	glycerolipids
CdM769	MAG (18 : 3) isomer 1	—	—	—	1.05×10^{0}	1.17×10^{-1}	Down	—	—	—	—	—	—	
CdM713	DGMG (18 : 1)	—	—	—	1.06×10^{0}	7.14×10^{-2}	Down	—	—	—	—	—	—	
CdM711	DGMG (18 : 2) isomer 2	—	—	—	1.07×10^{0}	7.23×10^{-2}	Down	—	—	—	—	—	—	
CdM767	MAG (18 : 3) isomer 4	—	—	—	1.08×10^{0}	1.05×10^{-1}	Down	—	—	—	—	—	—	
CdM168	Thymine	2.07×10^{0}	1.96×10^{4}	Up	—	—	—	2.75×10^{0}	1.97×10^{-5}	Down	—	—	—	Nucleotide
CdM161	8-Hydroxyguanosine	2.11×10^{0}	1.25×10^{4}	Up	—	—	—	2.59×10^{0}	9.92×10^{-5}	Down	—	—	—	and its
CdM183	5-Methyluridine	2.15×10^{0}	5.82×10^{-5}	Down	2.36×10^{0}	8.80×10^{-5}	Down	—	—	—	—	—	—	derivatives
CdM179	Guanosine 3′,5′-cyclic monophosphate	2.15×10^{0}	5.33×10^{-5}	Down	—	—	—	2.67×10^{0}	1.87×10^{4}	Up	—	—	—	
CdM127	Uracil	—	—	—	1.12×10^{0}	1.51×10^{-1}	Down	—	—	—	—	—	—	
CdM61	Cytidine 5′-monophosphate (cytidylic acid)	—	—	—	2.09×10^{0}	3.28×10^{-4}	Down	—	—	—	2.01×10^{0}	3.05×10^{3}	Up	
CdM73	Inosine	—	—	—	—	—	—	2.38×10^{0}	2.40×10^{3}	Up	—	—	—	
CdM18	2′-Deoxyinosine-5′-monophosphate	—	—	—	—	—	—	—	—	—	1.02×10^{0}	6.10×10^{1}	Up	
CdM74	iP7G	—	—	—	—	—	—	—	—	—	1.23×10^{0}	1.03×10^{-1}	Down	
CdM585	Sebacate	1.98×10^{0}	2.58×10^{-4}	Down	2.56×10^{0}	2.05×10^{-5}	Down	1.08×10^{0}	1.34×10^{-1}	Down	—	—	—	Organic
CdM242	Sinapoyl malate	2.04×10^{0}	6.47×10^{3}	Up	—	—	—	—	—	—	—	—	—	acids
CdM1091	*p*-Hydroxyphenyl acetic acid	2.25×10^{0}	7.00×10^{-6}	Down	—	—	—	—	—	—	—	—	—	
CdM1067	Mandelic acid	2.25×10^{0}	6.61×10^{-6}	Down	—	—	—	—	—	—	—	—	—	
CdM941	3-Hydroxybutyrate	2.26×10^{0}	1.73×10^{-5}	Down	—	—	—	—	—	—	—	—	—	
CdM328	4-Hydroxybenzoic acid	2.35×10^{0}	7.99×10^{-6}	Down	—	—	—	—	—	—	2.44×10^{0}	9.33×10^{4}	Up	
CdM1041	2-Methylglutaric acid	2.42×10^{0}	4.39×10^{-6}	Down	—	—	—	—	—	—	—	—	—	
CdM1040	Adipic acid	2.42×10^{0}	4.10×10^{-6}	Down	—	—	—	—	—	—	—	—	—	
CdM1042	5-Hydroxyhexanoic acid	—	—	—	1.12×10^{0}	1.26×10^{-1}	Down	—	—	—	1.20×10^{0}	1.28×10^{1}	Up	

Table 2 (*Contd.*)

		Saline-alkali land *vs.* grassland						Sandy land *vs.* saline-alkali land						
		Inflorescence (A1 *vs.* B1)			Succulent stem (A2 *vs.* B2)			Inflorescence (C1 *vs.* A1)			Succulent stem (C2 *vs.* A2)			
No.	Compounds	VIP	Fold change	Type	VIP	Fold change	Type	VIP	Fold change	Type	VIP	Fold change	Type	Class
CdM1051	2-Isopropylmalate	—	—	—	1.17×10^{0}	1.07×10^{-1}	Down	—	—	—	1.25×10^{0}	1.57×10^{1}	Up	
CdM1045	3-Hydroxyanthranilic acid	—	—	—	2.44×10^{0}	5.40×10^{-5}	Down	—	—	—	—	—	—	
CdM172	4-Acetamidobutyric acid	—	—	—	2.60×10^{0}	4.66×10^{-6}	Down	—	—	—	2.49×10^{0}	2.15×10^{5}	Up	
CdM577	*N*′,*N*″-*p*-Coumaroyl-feruloyl putrescine	1.89×10^{0}	3.68×10^{-4}	Down	—	—	—	2.34×10^{0}	2.72×10^{3}	Up	—	—	—	Phenola-mides
CdM394	*N*′,*N*″-Diferuloylspermidine	2.11×10^{0}	8.25×10^{-5}	Down	—	—	—	2.61×10^{0}	1.21×10^{4}	Up	—	—	—	
CdM216	*N*-*p*-Coumaroyl putrescine	2.44×10^{0}	3.35×10^{-6}	Down	—	—	—	3.03×10^{0}	2.99×10^{5}	Up	—	—	—	
CdM217	*N*′-*p*-Coumaroyl putrescine	2.45×10^{0}	2.95×10^{-6}	Down	—	—	—	3.04×10^{0}	3.39×10^{5}	Up	—	—	—	
CdM365	*N*′,*N*″-Di-*p*-coumaroylspermidine	2.58×10^{0}	8.26×10^{-7}	Down	—	—	—	1.45×10^{0}	1.67×10^{1}	Up	—	—	—	
CdM351	*N*′,*N*″-feruloyl-caffeoylspermidine	—	—	—	2.25×10^{0}	2.17×10^{-4}	Down	—	—	—	—	—	—	
CdM1312	Gibberellin A4 (GA4)	1.72×10^{0}	1.57×10^{-3}	Down	—	—	—	—	—	—	—	—	—	Phyto-hormones
CdM1334	Gibberellin A15	1.86×10^{0}	1.77×10^{3}	Up	2.24×10^{0}	1.90×10^{-4}	Down	2.42×10^{0}	2.70×10^{-4}	Down	2.14×10^{0}	5.25×10^{3}	Up	
CdM707	Gibberellin A9	2.09×10^{0}	5.87×10^{-5}	Down	—	—	—	—	—	—	2.40×10^{0}	3.50×10^{4}	Up	
CdM1292	(+)-Jasmonic acid (JA)	2.09×10^{0}	9.51×10^{-5}	Down	—	—	—	2.60×10^{0}	1.05×10^{4}	Up	—	—	—	
CdM606	Gibberellin A20	2.16×10^{0}	3.01×10^{-5}	Down	—	—	—	2.67×10^{0}	3.32×10^{4}	Up	2.46×10^{0}	6.12×10^{4}	Up	
CdM278	Indole carboxylic acid	2.16×10^{0}	2.03×10^{4}	Up	—	—	—	2.79×10^{0}	1.80×10^{-5}	Down	—	—	—	
CdM248	*trans*-Zeatin 9-*O*-glucoside	—	—	—	1.16×10^{0}	1.04×10^{-1}	Down	—	—	—	—	—	—	
CdM1001	5-*O*-Feruloyl quinic acid glucoside	1.78×10^{0}	8.36×10^{2}	Up	—	—	—	—	—	—	—	—	—	Quinate and its derivatives
CdM1003	3-*O*-Feruloyl quinic acid glucoside	1.83×10^{0}	1.22×10^{3}	Up	—	—	—	—	—	—	—	—	—	
CdM315	3-*O*-Feruloyl quinic acid	1.95×10^{0}	2.98×10^{3}	Up	2.22×10^{0}	3.51×10^{3}	Up	2.49×10^{0}	1.96×10^{-4}	Down	—	—	—	
CdM1108	3-*O*-*p*-Coumaroyl quinic acid	2.01×10^{0}	1.47×10^{-4}	Down	2.25×10^{0}	1.90×10^{-4}	Down	—	—	—	2.15×10^{0}	5.27×10^{3}	Up	
CdM289	Chlorogenic acid (3-*O*-caffeoylquinic acid)	2.05×10^{0}	1.44×10^{-4}	Down	—	—	—	2.54×10^{0}	6.92×10^{3}	Up	—	—	—	
CdM1028	5-*O*-*p*-Coumaroyl shikimic acid *O*-hexoside	2.05×10^{0}	6.71×10^{-5}	Down	—	—	—	—	—	—	—	—	—	
CdM1079	3-*O*-*p*-Coumaroyl shikimic acid *O*-hexoside	2.07×10^{0}	9.14×10^{3}	Up	—	—	—	—	—	—	2.21×10^{0}	1.06×10^{-4}	Down	
CdM411	Chlorogenic acid methyl ester	2.49×10^{0}	5.36×10^{5}	Up	—	—	—	—	—	—	—	—	—	
CdM1056	*O*-*p*-Coumaroyl quinacyl quinic acid *O*-hexoside	—	—	—	—	—	—	—	—	—	1.19×10^{0}	4.97×10^{-2}	Down	

[a] Note: A1: inflorescence in saline-alkali land, A2: succulent stem in saline-alkali land, B1: inflorescence in grassland, B2: succulent stem in grassland, C1: inflorescence in sandy land, and C2: succulent stem in sandy land.

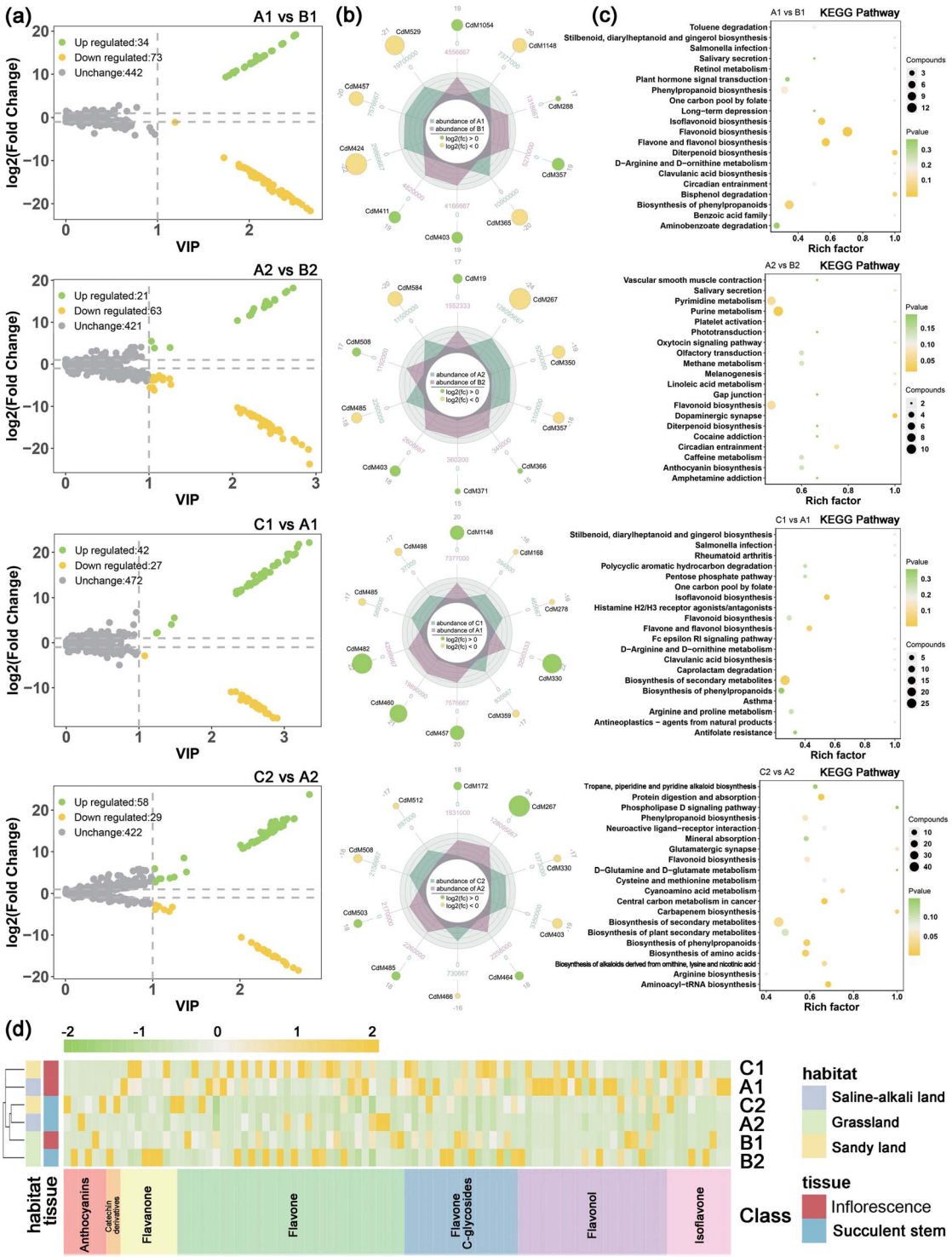

Fig. 3 Differential metabolite features related to salt-alkali stress of *C. deserticola* in inflorescence and succulent stem. (a) Volcano map related to saline-alkali stress; the yellow dots represent downregulated differentially expressed metabolites, the green dots represent upregulated differentially expressed metabolites, and the gray dots represent metabolites detected but not significantly different. (b) The radar charts showed the top 10 differential metabolites related to saline-alkali stress. The number in the middle of each branch is the relative content, and the number in each circle is the $\log_2$ foldchange value. (c) KEGG pathway enrichment results of differential metabolites related to saline-alkali stress. The rich factor is the ratio of the number of differentially expressed metabolites in the pathway to the total number of metabolites annotated by the pathway. The larger the value, the greater the degree of enrichment. The closer the *p*-value is to 0, the more significant the enrichment. The size of the dot in the figure represents the number of significantly different metabolites enriched in the corresponding pathway. (d) Hierarchical clustering analysis for the identification of different metabolites of flavonoids related to salt-alkali stress. Yellow represents relatively high content, and the green represents relatively low content. A1: inflorescence in saline-alkali land, A2: succulent stem in saline-alkali land, B1: inflorescence in grassland, B2: succulent stem in grassland, C1: inflorescence in sandy land, and C2: succulent stem in sandy land.

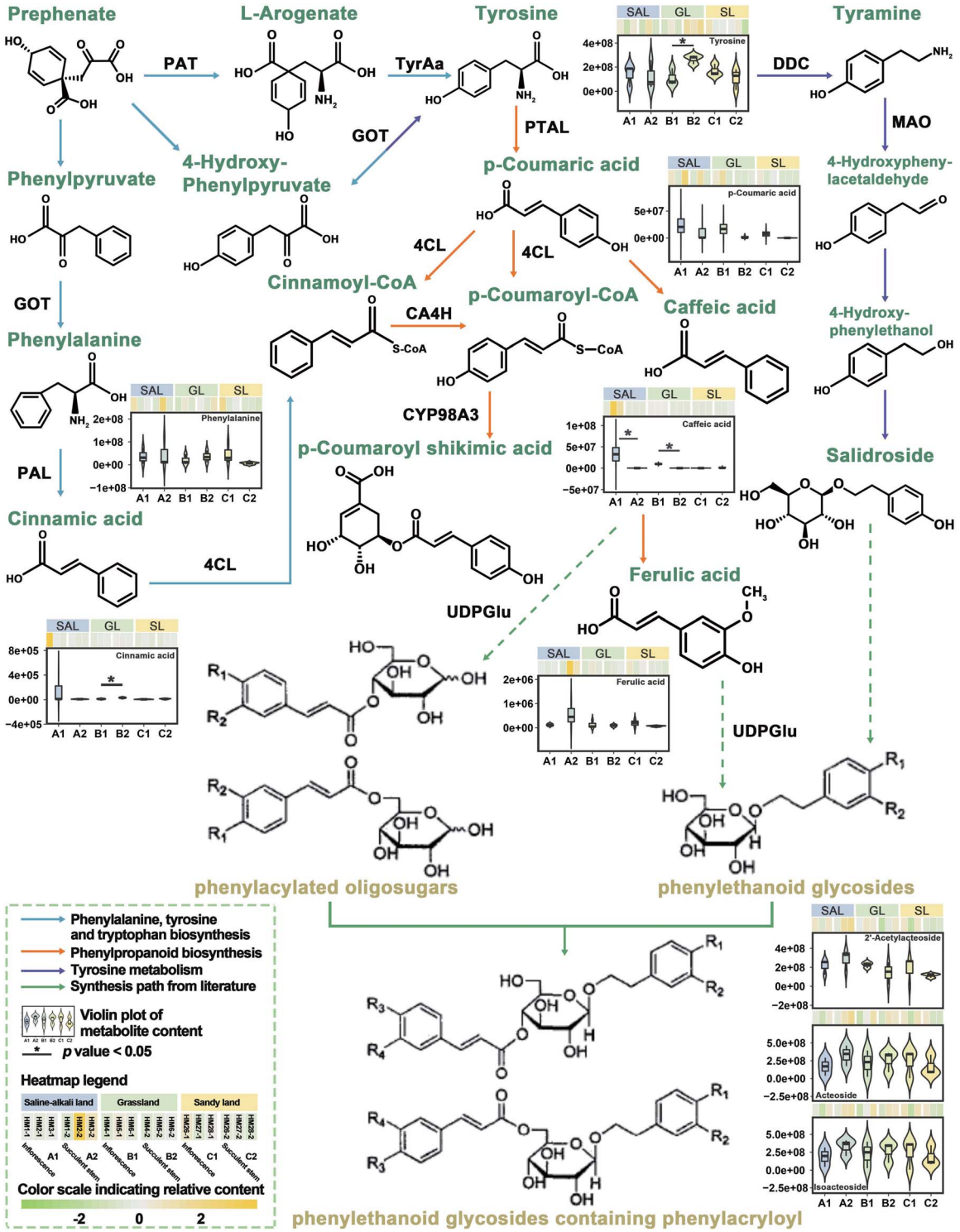

Fig. 4 Metabolites pathways involved in the biosynthesis of PhGs of the inflorescence and succulent stem of *C. deserticola* in three ecotypes. The blue arrows represent the phenylalanine, tyrosine, and tryptophan biosynthetic pathway. The orange arrow represents the phenylpropanoid biosynthetic pathway. The purple arrow represents the tyrosine metabolic pathway. The green arrow represents the pathway from literature. The violin plot and heatmap showing the content of the change of detected metabolites. Aspartate aminotransferase (*GOT*/*PAT*, EC: 2.6.1.1), Phenylalanine ammonia-lyase (*PAL*, EC: 4.3.1.24), 4-coumarate-CoA ligase (*4CL*, EC: 6.2.1.12), 5-*O*-(4-coumaroyl)-D-quinate 3′-monooxygenase (*CYP98A3*, EC: 1.14.14.96), arogenate dehydrogenase (*TyrAa*, EC 1.3.1.78), phenylalanine/tyrosine ammonia-lyase (*PTAL*, EC 4.3.1.25), diaminobutyrate-2-oxoglutarate transaminase (*DDC*, EC 2.6.1.76), monoamine oxidase (*MAO*, EC 1.4.3.4), *trans*-cinnamate 4-monooxygenase (*CA4H*, EC 1.14.14.91). A1: inflorescence in saline-alkali land, A2: succulent stem in saline-alkali land, B1: inflorescence in grassland, B2: succulent stem in grassland, C1: inflorescence in sandy land, and C2: succulent stem in sandy land.

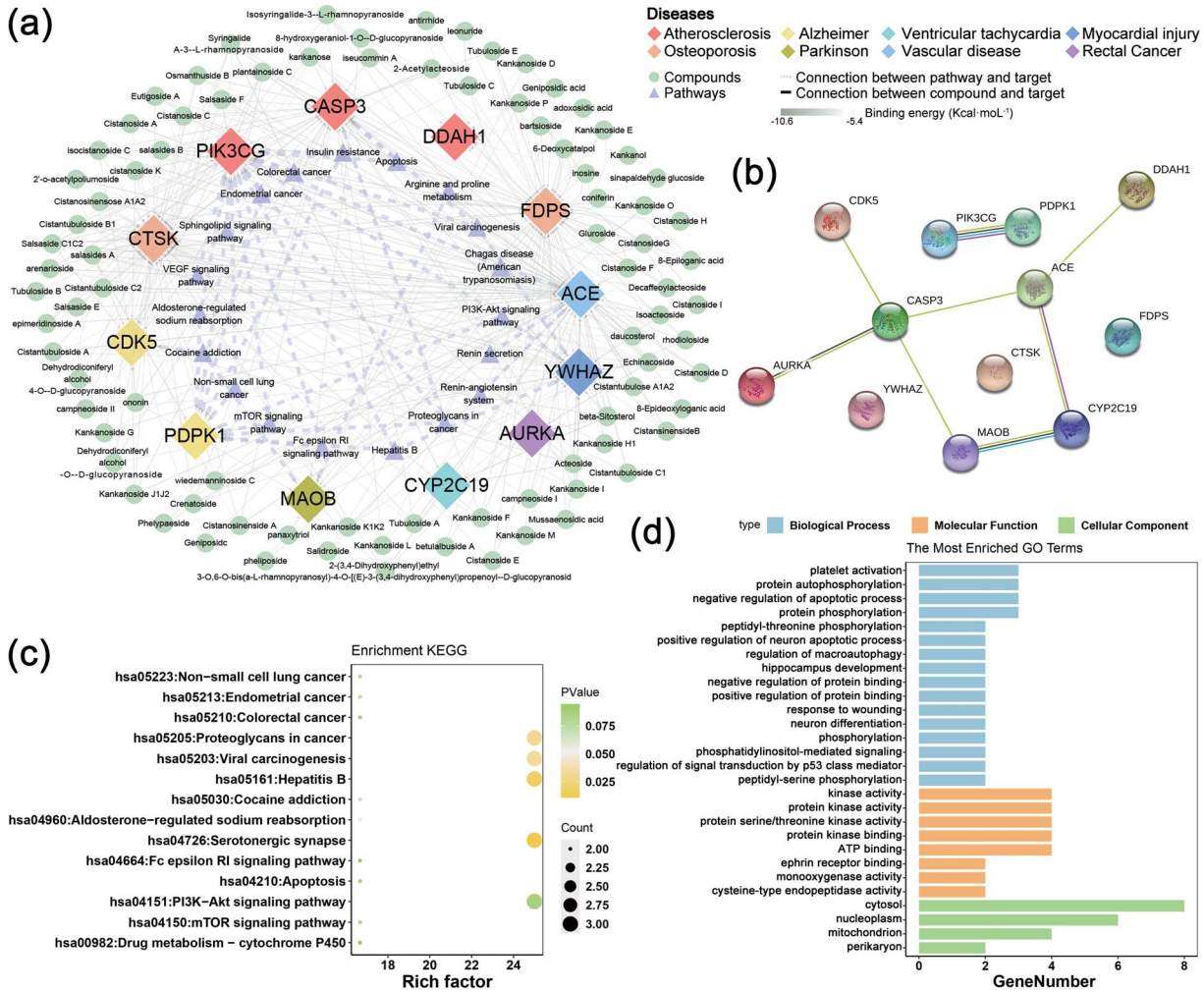

Fig. 5 Molecular docking for uncovering the multiple mechanisms of *C. deserticola* against diseases. (a) Simulation of a potential target-compounds-pathway docking network. Target genes by diamond (magenta), diamonds of the same color represent the same disease. Compounds by circles (orange), and pathways by triangles (red). The color of the connection line between the compound and the target gene showing the result of the free energy of molecular docking. The closer the color is to green, the smaller the free energy and the better the effect of the compound. (b) Visualization of the protein–protein interaction (PPI) of the 12 target genes using STRING and Cytoscape databases. (c) Bubble graph demonstrating statistically significant pathways that include the 12 genes analyzed using the KEGG database. The rich factor is the ratio of the number of differentially expressed metabolites in the pathway to the total number of metabolites annotated by the pathway. The larger the value, the greater the degree of enrichment. The closer the p-value is to 0, the more significant the enrichment. The size of the dot in the figure represents the number of significantly different metabolites enriched in the corresponding pathway. (d) GO analysis of target–disease gene interactions for major active components of *C. deserticola* to reveal the related biological process (BP), cellular component (CC), and (c) molecular function (MF).

results of literature comparison and molecular docking, 15 targets and 88 compounds were finally screened (Tables S2 and S3†). Table S2† showed information about targets, diseases, and predicted genes. In order to further understand the comprehensive relationship between the selected compounds, selected predicted genes, and diseases, a comprehensive network analysis was performed using Cytoscape version 3.7.0 (Fig. 5a). An intricate network was formed among the selected compounds and their potential targets regarding osteoporosis, vascular disease, atherosclerosis, myocardial injury, Alzheimer disease, Parkinson, ventricular tachycardia, and rectal cancer. The degree of the network on the compound–target interaction was depicted in Table S2,† which indicated that the predicted genes *CTSK* and *FDPS* related to osteoporosis, and the target gene *ACE* related to vascular disease have a higher degree value, indicating that more compounds in *C. deserticola* can act on these targets gene.

The interaction between the 12 genes was analyzed and visualized using STRING databases. The protein–protein interaction (PPI) network (Fig. 5b) was constructed under "medium confidence (0.4 by default)". Using the DAVID database, the 14 KEGG pathways of the 12 predicted genes were visualized in Fig. 5c. The KEGG pathways enriched by these predicted genes mainly include serotonergic synapse, hepatitis B, proteoglycans in cancer, and viral carcinogenesis. The list of the 12 screened predicted genes was uploaded to the DAVID database for GO

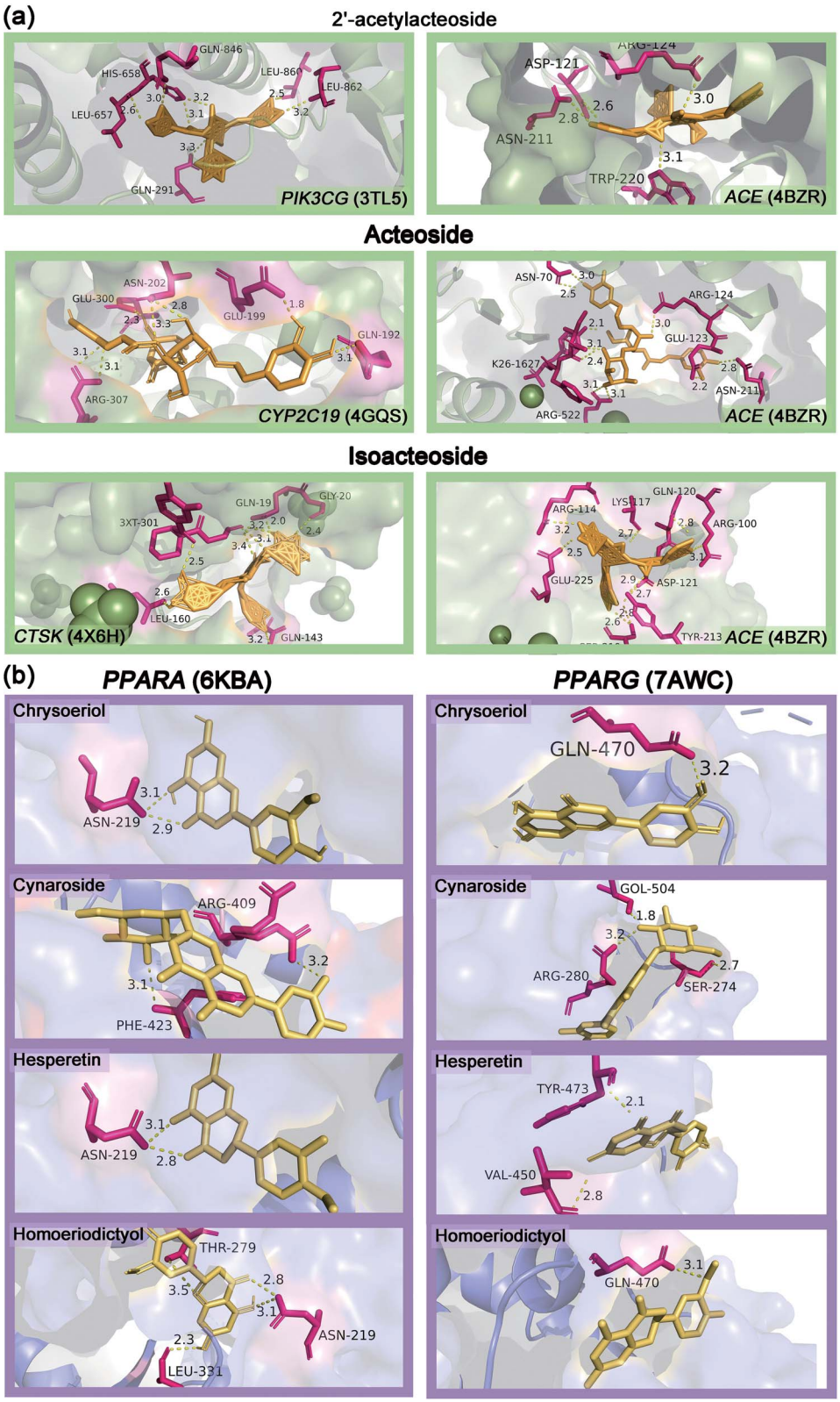

Fig. 6 (a) Predicted binding mode of 2′-acetylacteoside, acteoside and isoacteoside with targets in three-dimensions (3D). 2′-acetylacteoside: vascular disease (4BZR) and atherosclerosis (3TL5); acteoside: vascular disease (4BZR) and ventricular tachycardia (4GQS); isoacteoside: vascular disease (4BZR) and osteoporosis (4X6H). (b) Molecular docking analysis in the inflorescence of *C. deserticola*, predicted binding mode of unique metabolites in inflorescence with important targets related to inflammation in three-dimensions (3D).

enrichment analysis (Fig. 5d). The targets were involved in many biological processes (BP) including "platelet activation", "positive regulation of neuron apoptotic process", and "hippocampus development". "Cytosol", "nucleoplasm", and "mitochondrion" ranked the highest in the cellular component (CC) category, while "kinase activity", "protein kinase activity", and "protein serine/threonine kinase activity" were the primary molecular function (MF) involved.

Table S3† showed the molecular docking results of the effective components of succulent stems of *C. deserticola* and disease targets. As shown in Fig. 4, 2′-acetylacteoside, acteoside and isoacteoside in PhGs of *C. deserticola* respond to salt-alkali stress. Fig. 6a and S4a† demonstrated a detailed view of the molecular docking of these three compounds with high-scoring targets. 2′-Acetylacteoside had excellent docking with targets related to atherosclerosis (3TL5) and vascular disease (4BZR). Isoacteoside had high score docking with targets related to osteoporosis (4X6H) and vascular disease (4BZR). Acteoside had better docking with targets related to vascular disease (4BZR) and ventricular tachycardia (4GQS). Fig. 6b and S4b† showed the results of molecular docking between four flavonoids detected only in the inflorescence and the selected inflammation targets. Table S4† indicated that chrysoeriol and cynaroside had higher scores with 2 targets.

4. Discussion

Our study indicates the inflorescence of *C. deserticola* not only contains the main active ingredient PhGs, but also contains a large number of flavonoids. In particular, the relative content of flavonoids are significantly higher than the succulent stems. Flavonoids, due to their antioxidant, anti-cancer properties, anti-inflammatory and anti-mutagenic properties, and their ability to regulate the function of key cell enzymes, are now considered as an essential ingredient in various health foods, medicines, drugs, and cosmetics applications.[32] Flavonols are a class of flavonoids with a 3-hydroxyflavonoid skeleton (IUPAC name: 3-hydroxy-2-phenylchromium-4-one). Their diversity stems from the different positions of the phenol-OH group.[33] The tautomerism of flavonols causes double fluorescence (due to excited-state intramolecular proton transfer or ESIPT), which can promote UV protection in plants.[34] Therefore, we recommend reusing the inflorescences of *C. deserticola* rich in flavonoids rather than discarding them.

Interestingly, we found that most of the differential metabolites associated with saline-alkali stress in the three ecotypes of *C. deserticola* were also flavonoids. Our previous research[16] found that the relative content of phenylethanoid glycosides (PhGs) in the succulent stems of *C. deserticola* (saline-alkali land) is higher than the other two ecotypes. Salinity can cause a variety of adverse effects in plants, and one of its inevitable consequences is the excessive production of reactive oxygen species (ROS). Fini *et al.* believed that flavonoids are an important part of the secondary ROS scavenging system.[35] Xumei Jia *et al.* speculated that sucrose signaling regulates ROS homeostasis by inducing phenylpropane biosynthesis pathway and flavonoid synthesis.[36] Wang *et al.* believe that because flavonoids can remove harmful stress response substances (including free radicals, singlet oxygen molecules, and peroxides), they can enhance the tolerance of plants to abiotic and biotic stresses.[37] Zhang *et al.* used transcriptome analysis to reveal that the molecular response of *Cynanchum auriculatum* leaves to salt stress. They found that the biosynthetic pathway of flavonoids and phenylpropanoids was activated. In this pathway, *trans*-cinnamic acid 4-monooxygenase (*C4H*) and chalcone isomers directly related to the synthesis of flavonoids, in which the expression levels of them were all up-regulated. These results indicated that more flavonoids were synthesized, which may contribute to the total antioxidant capacity in response to the saltwater stress of *C. auriculatum*. Similarly, Walia *et al.* reported that a large number of genes in the flavonoid biosynthesis pathway were up-regulated under salt stress, which played an important protective role in resisting salt stress.[38] In summary, we believe that saline-alkali stress promotes the accumulation of flavonoids in both succulent stems and inflorescences of *C. deserticola*. We strongly regard saline soil as the best soil type for *C. deserticola* cultivation.

On the one hand, we obtained the unique flavonoids in the inflorescence by analyzing the results of the metabolome. Considering the role of flavonoids in anti-inflammatory, we carried out molecular docking analysis of these five compounds with inflammation-related targets, so as to provide guidance for the development of non-medicinal inflorescence resources. On the other hand, we carried out molecular docking of the active components of the succulent stems of *C. deserticola* to make up for the gap in this regard. It provided some directions for the therapeutic mechanism of the active ingredients of *C. deserticola* for the treatment of aging diseases. Zhang *et al.* found that *C. deserticola* extract has potential anti-osteoporosis activity, and this effect is at least partly involved in RANKL/RANK/TRAF6 mediated NF-κB and PI3K/AKT signal transduction and the regulation of c-Fos and NFAT2 levels.[39] The published data proved that several isolated compounds of *C. deserticola*, including echinacoside, acteoside, and cistanoside A, were also reported to be processing anti-osteoporosis activities.[40–42] Compounds associated with atherosclerosis-related targets include 2′-acetylacteoside, acteoside, echinacoside, daucosterol, isoacteoside, cistanoside A, arenarioside, cistanosinenside A, *etc.* Though more biological validation is needed to further validate the current results, this work may provide new treatment opportunities for aging diseases such as osteoporosis, atherosclerosis, *etc.*, and may open up new ways for the discovery of drug combinations from the natural products of *C. deserticola*.

In conclusion, this study is the first to reveal the metabolic variation characteristics between the inflorescences and succulent stems of the three ecotypes of *C. deserticola*. Moreover, molecular docking was applied to screen the potential therapeutic targets and compounds of *C. deserticola*. The following conclusions were obtained: (1) the number of metabolites in the inflorescence is more abundant than that of the succulent stems, and most of the metabolites only detected in the inflorescence are flavonoids, which can be used as a material for the development of new medicinal resources. (2)

Isorhamnetin *O*-hexoside and rosinidin *O*-hexoside can be used as chemical markers to distinguish succulent stems and inflorescences in the three ecotypes. (3) Saline-alkali stress leads to a large accumulation of flavonoids in *C. deserticola*. We suggest that saline-alkali land is a good choice for cultivating *C. deserticola*. (4) The active ingredients of *C. deserticola* have good potential therapeutic effects on aging diseases such as osteoporosis and vascular disease and atherosclerosis. Meanwhile, the unique flavonoids in the inflorescence of *C. deserticola* have high docking scores with the anti-inflammatory targets, which provides a new direction for the development and utilization of the inflorescence. This research has laid a theoretical foundation for the artificial cultivation and effective resource development of *C. deserticola*. Our study provides novel methods and theoretical guidance for the development and utilization of new resources of medicinal plants and the discovery of potential therapeutic mechanisms of natural products.

Funding

This work was supported by National Natural Science Foundation of China (81473315 and U1812403-1), National Science & Technology Fundamental Resources Investigation Program of China (2018FY100701), the Open Research Fund of Chengdu University of Traditional Chinese Medicine Key Laboratory of Systematic Research of Distinctive Chinese Medicine Resources in Southwest China (003109034001) and Beijing Natural Scientific Foundation (7202135), which are gratefully acknowledged.

Author contributions

All authors contributed to manuscript revision, read and approved the submitted version. XS, LF-H and YZ contributed conception and design of the study; XS, PJ and BA collected the samples; XS and YZ organized the database; XS performed the statistical analysis; XS and LF-H wrote the first draft of the manuscript; LF-H, YZ, JP and AB wrote sections of the manuscript.

Conflicts of interest

The authors declare no conflict of interest.

Acknowledgements

We express our great thanks to Xiang Zhang from the Institute of Medicinal Plant Development, Chinese Academy of Medical Sciences, Peking Union Medical College, for the guidelines for molecular docking.

References

1 T. Wang, X. Zhang and W. Xie, *Am. J. Chin. Med.*, 2012, **40**, 1123–1141.
2 Y. Jiang and P. F. Tu, *J. Chromatogr. A*, 2009, **1216**, 1970–1979.
3 L. Gu, W.-T. Xiong, C. Wang, H.-X. Sun, G.-F. Li and X. Liu, *Asian J. Androl.*, 2013, **15**, 838.
4 N. A. Stefanova, A. Z. Fursova, K. N. Sarsenbaev and N. G. Kolosova, *J. Ethnopharmacol.*, 2011, **138**, 624–632.
5 C. Gu, X. Yang and L. Huang, *Front. Pharmacol.*, 2016, **7**, 289.
6 S. Zheng, X. Jiang, L. Wu, Z. Wang and L. Huang, *PLoS One*, 2014, **9**, e98061.
7 X. J. Qin, W. Ni, C. X. Chen and H. Y. Liu, *Nat. Prod. Bioprospect.*, 2018, **8**, 265–278.
8 F. Yang, Y. Qi, W. Liu, J. Li, D. Wang, L. Fang and Y. Zhang, *Molecules*, 2019, **24**(19), 3448.
9 H. L. Qiao, P. F. Lu, R. Xu, J. Chen, X. Wang, W. S. Ma and T. N. Liu, *Zhongyaocai*, 2012, **35**, 573–577.
10 X. Peng, Y. Luo, J. Wang, T. Ji, L. Yuan and G. Kai, *Food Res. Int.*, 2020, **138**, 109799.
11 E. Gemperline, C. Keller and L. Li, *Anal. Chem.*, 2016, **88**, 3422–3434.
12 B. Worley and R. Powers, *Curr. Metabolomics*, 2013, **1**, 92–107.
13 S. Wei, X. Yang, G. Huo, G. Ge, H. Liu, L. Luo, J. Hu, D. Huang and P. Long, *Int. J. Mol. Sci.*, 2020, **21**, 1481.
14 J. Xu, J. Yan, W. Li, Q. Wang, C. Wang, J. Guo, D. Geng, Q. Guan and F. Ma, *Int. J. Mol. Sci.*, 2020, **21**, 4797.
15 W. Xin, L. Zhang, W. Zhang, J. Gao, J. Yi, X. Zhen, M. Du, Y. Zhao and L. Chen, *Int. J. Mol. Sci.*, 2019, **20**, 5893.
16 X. Sun, L. Li, J. Pei, C. Liu and L.-F. Huang, *Plant Mol. Biol.*, 2020, **102**, 253–269.
17 W. Liu, Q. Song, Y. Cao, N. Xie, Z. Li, Y. Jiang, J. Zheng, P. Tu, Y. Song and J. Li, *J. Pharm. Biomed. Anal.*, 2019, **162**, 16–27.
18 P. Zou, Y. Song, W. Lei, J. Li, P. Tu and Y. Jiang, *Acta Pharm. Sin. B*, 2017, **7**, 647–656.
19 S. Li and B. Zhang, *Chin. J. Nat. Med.*, 2013, **11**, 110–120.
20 X. Zhang, D. Wang, X. Ren, A. G. Atanasov, R. Zeng and L. Huang, *Curr. Protein Pept. Sci.*, 2019, **20**, 964–975.
21 W. Wu, Z. Zhang, F. Li, Y. Deng, M. Lei, H. Long, J. Hou and W. Wu, *Int. J. Mol. Sci.*, 2020, **21**, 1766.
22 J. Liu, J. Zhu, J. Xue, Z. Qin, F. Shen, J. Liu, X. Chen, X. Li, Z. Wu, W. Xiao, C. Zheng and Y. Wang, *Sci. Rep.*, 2017, **7**, 16364.
23 Y. Q. Li, Y. Chen, J. Y. Fang, S. Q. Jiang, P. Li and F. Li, *J. Ethnopharmacol.*, 2020, **254**, 112764.
24 L. Gu, W. T. Xiong, C. Wang, H. X. Sun, G. F. Li and X. Liu, *Asian J. Androl.*, 2013, **15**, 838–840.
25 Z. Li, H. Lin, L. Gu, J. Gao and C. M. Tzeng, *Front. Pharmacol.*, 2016, **7**, 41.
26 T. Wang, X. Zhang and W. Xie, *Am. J. Chin. Med.*, 2012, **40**, 1123–1141.
27 J. Stamos, M. X. Sliwkowski and C. Eigenbrot, *J. Biol. Chem.*, 2002, **277**, 46265–46272.
28 P. A. Harris, M. Cheung, R. N. Hunter, 3rd, M. L. Brown, J. M. Veal, R. T. Nolte, L. Wang, W. Liu, R. M. Crosby, J. H. Johnson, A. H. Epperly, R. Kumar, D. K. Luttrell and J. A. Stafford, *J. Med. Chem.*, 2005, **48**, 1610–1619.
29 J. Cheung, M. J. Rudolph, F. Burshteyn, M. S. Cassidy, E. N. Gary, J. Love, M. C. Franklin and J. J. Height, *J. Med. Chem.*, 2012, **55**, 10282–10286.
30 M. Kožíšek, M. Lepšík, K. Grantz Šašková, J. Brynda, J. Konvalinka and P. Rezáčová, *FEBS J.*, 2014, **281**, 1834–1847.

31 D. Szklarczyk, A. L. Gable, D. Lyon, A. Junge, S. Wyder, J. Huerta-Cepas, M. Simonovic, N. T. Doncheva, J. H. Morris, P. Bork, L. J. Jensen and C. V. Mering, *Nucleic Acids Res.*, 2019, **47**, D607–D613.
32 A. Panche, A. Diwan and S. Chandra, *J. Nutr. Sci.*, 2016, **5**, e47.
33 J. B. Harborne and C. A. Williams, *The flavonoids*, Springer, 1975, pp. 376–441.
34 G. J. Smith and K. R. Markham, *J. Photochem. Photobiol., A*, 1998, **118**, 99–105.
35 A. Fini, C. Brunetti, M. Di Ferdinando, F. Ferrini and M. Tattini, *Plant Signaling Behav.*, 2011, **6**, 709–711.
36 X. M. Jia, Y. F. Zhu, Y. Hu, R. Zhang, L. Cheng, Z. L. Zhu, T. Zhao, X. Zhang and Y. X. Wang, *Hortic. Res.*, 2019, **6**, 91.
37 F. Wang, W. Kong, G. Wong, L. Fu, R. Peng, Z. Li and Q. Yao, *Mol. Genet. Genomics*, 2016, **291**, 1545–1559.
38 H. Walia, C. Wilson, P. Condamine, X. Liu, A. M. Ismail, L. Zeng, S. I. Wanamaker, J. Mandal, J. Xu, X. Cui and T. J. Close, *Plant Physiol.*, 2005, **139**, 822–835.
39 B. Zhang, L.-L. Yang, S.-Q. Ding, J.-J. Liu, Y.-H. Dong, Y.-T. Li, N. Li, X.-J. Zhao, C.-L. Hu and Y. Jiang, *Front. Pharmacol.*, 2019, **10**, 1412.
40 F. Li, X. Yang, Y. Yang, C. Guo, C. Zhang, Z. Yang and P. Li, *Phytomedicine*, 2013, **20**, 549–557.
41 S.-Y. Lee, K.-S. Lee, S. H. Yi, S.-H. Kook and J.-C. Lee, *PLoS One*, 2013, **8**, e80873.
42 X. Xu, Z. Zhang, W. Wang, H. Yao and X. Ma, *Molecules*, 2017, **22**, 197.